Interferon-responsive intestinal BEST4/CA7+ cells are targets of bacterial diarrheal toxins

Wang, Daisong; Spoelstra, Willem Kasper; Lin, Lin; Akkerman, Ninouk; Krueger, Daniel; Dayton, Talya; van Zon, Jeroen S.; Tans, Sander J.; van Es, Johan H.; Clevers, Hans

DOI
10.1016/j.stem.2025.02.003

Publication date
2025

Document Version
Final published version

Published in
Cell Stem Cell

Citation (APA)
Wang, D., Spoelstra, W. K., Lin, L., Akkerman, N., Krueger, D., Dayton, T., van Zon, J. S., Tans, S. J., van Es, J. H., & Clevers, H. (2025). Interferon-responsive intestinal BEST4/CA7+ cells are targets of bacterial diarrheal toxins. *Cell Stem Cell*, *32*(4), 598-612.e5. https://doi.org/10.1016/j.stem.2025.02.003

Cell Stem Cell

Article

Interferon-responsive intestinal BEST4/CA7$^+$ cells are targets of bacterial diarrheal toxins

Graphical abstract

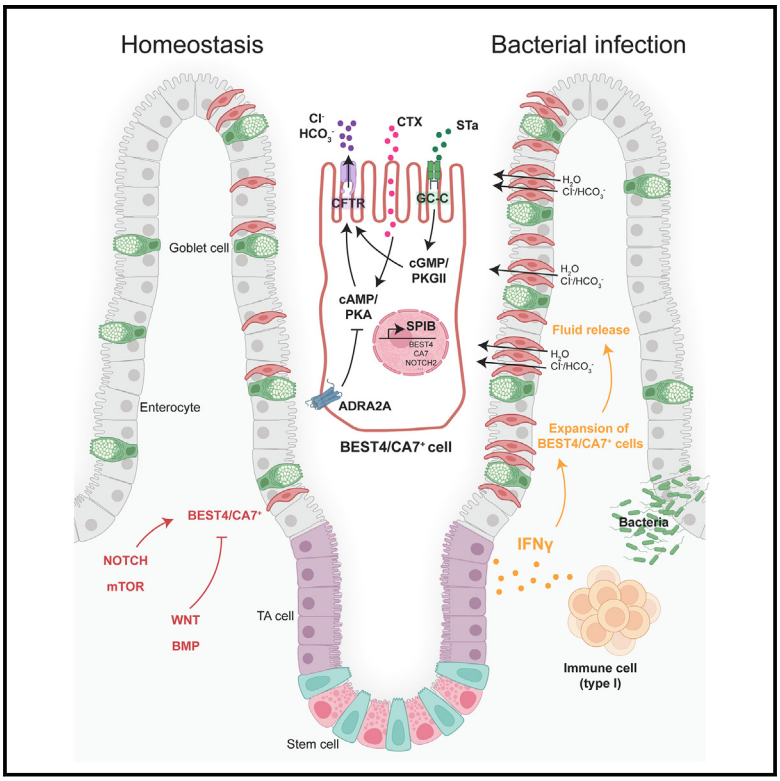

Highlights

- A human intestinal organoid model containing BEST4/CA7$^+$ cells is established
- BEST4/CA7$^+$ cell differentiation requires Notch signaling and transcription factor SPIB
- IFN-γ induces expansion of BEST4/CA7$^+$ cell pool
- Small-intestinal BEST4/CA7$^+$ cells control electrolyte/fluid homeostasis through CFTR

Authors

Daisong Wang, Willem Kasper Spoelstra, Lin Lin, ..., Sander J. Tans, Johan H. van Es, Hans Clevers

Correspondence

h.clevers@hubrecht.eu

In brief

Clevers and colleagues investigated the differentiation and function of human BEST4/CA7$^+$ cells using *in vitro* intestinal organoid models, which help reveal these cells' responses to various niche factors, cytokines, and bacterial toxins, as well as their key roles in electrolyte homeostasis.

Wang et al., 2025, Cell Stem Cell *32*, 598–612
April 3, 2025
https://doi.org/10.1016/j.stem.2025.02.003

CellPress

CellPress
OPEN ACCESS

Cell Stem Cell

Article

Interferon-responsive intestinal BEST4/CA7$^+$ cells are targets of bacterial diarrheal toxins

Daisong Wang,[1,2] Willem Kasper Spoelstra,[3] Lin Lin,[1,2,4] Ninouk Akkerman,[1,2,6] Daniel Krueger,[1,2] Talya Dayton,[1,2,7] Jeroen S. van Zon,[3] Sander J. Tans,[3,5] Johan H. van Es,[1,2] and Hans Clevers[1,2,4,6,8,*]

[1]Hubrecht Institute, Royal Netherlands Academy of Arts and Sciences (KNAW) and UMC Utrecht, Utrecht 3584 CT, the Netherlands
[2]Oncode Institute, Hubrecht Institute, Utrecht 3584 CT, the Netherlands
[3]AMOLF, Amsterdam 1009 DB, the Netherlands
[4]The Princess Máxima Center for Pediatric Oncology, Utrecht 3584 CS, the Netherlands
[5]Department of Bionanoscience, Kavli Institute of Nanoscience Delft, Delft University of Technology, Delft 2629 HZ, the Netherlands
[6]Present address: Institute of Human Biology (IHB), Pharma, Research and Early Development (pRED) of F. Hoffmann-La Roche Ltd., Basel, Switzerland
[7]Present address: Tissue Biology and Disease Modeling Unit, European Molecular Biology Lab, Barcelona, Spain
[8]Lead contact
*Correspondence: h.clevers@hubrecht.eu
https://doi.org/10.1016/j.stem.2025.02.003

SUMMARY

BEST4/CA7$^+$ cells of the human intestine were recently identified by single-cell RNA sequencing. While their gene expression profile predicts a role in electrolyte balance, BEST4/CA7$^+$ cell function has not been explored experimentally owing to the absence of BEST4/CA7$^+$ cells in mice and the paucity of human *in vitro* models. Here, we establish a protocol that allows the emergence of BEST4/CA7$^+$ cells in human intestinal organoids. Differentiation of BEST4/CA7$^+$ cells requires activation of Notch signaling and the transcription factor SPIB. BEST4/CA7$^+$ cell numbers strongly increase in response to the cytokine interferon-γ, supporting a role in immunity. Indeed, we demonstrate that BEST4/CA7$^+$ cells generate robust CFTR-mediated fluid efflux when stimulated with bacterial diarrhea-causing toxins and find the norepinephrine-ADRA2A axis as a potential mechanism in blocking BEST4/CA7$^+$ cell-mediated fluid secretion. Our observations identify a central role of BEST4/CA7$^+$ cells in fluid homeostasis in response to bacterial infections.

INTRODUCTION

BEST4/CA7$^+$ cells represent a small fraction of human intestinal epithelial cells. They were recently identified as specialized enterocytes through high-throughput single-cell RNA sequencing (scRNA-seq) and are defined by signature genes such as *BEST4*, *SPIB*, *CA7*, and *CFTR*.[1–6] Properties of BEST4/CA7$^+$ cells have been predicted based on their gene expression profile: the expression of *BEST4* and *CFTR*, which both encode Cl^-/HCO_3^- channels,[7,8] predicts a function in anion transport, while the expression of *OTOP2*, a proton-conducting ion channel,[9] suggests that these cells may sense acid.[6] To date, differentiation and function of BEST4/CA7$^+$ cells have not been studied experimentally as the mouse intestine does not harbor a BEST4/CA7$^+$ cell counterpart,[10] and stable *in vitro* models of human BEST4/CA7$^+$ cells have not been described.

Bacterial diarrheal toxins cause an imbalance of ion absorption or secretion across the gut epithelium, resulting in the movement of water to restore appropriate ion concentrations.[11] CFTR, a Cl^-/HCO_3^- channel, is among the best-known targets of diarrhea-causing pathogens through a variety of mechanisms.[7,11] Given the small numbers of BEST4/CA7$^+$ cells in gut epithelium, it has remained unclear whether these cells, as *CFTR*-high expressers, directly contribute to the ion homeostasis and whether their numbers increase in response to the signals induced by bacterial infections. In this study, we investigate the properties of BEST4/CA7$^+$ cells by creating genetically modified human intestinal organoid models and identify the BEST4/CA7$^+$ cells as a type 1 immune-responsive cell type that controls electrolyte/fluid homeostasis and represents a cellular target of bacterial diarrheal toxins in human intestine.

RESULTS

A human intestinal organoid model containing BEST4/CA7$^+$ cells

The originally described human intestinal organoids are cultured with a defined set of growth factors (Figure 1A, referred to as "expansion medium") to maintain long-term self-renewing stem cells and transient amplifying (TA) cells.[12] These conditions only allow limited differentiation of the various cell lineages.[13] To define culture conditions for organoids containing BEST4/CA7$^+$ cells, we removed the self-renewal factors (i.e., surrogate WNT,[14] Noggin, EGF, A83-01, SB202190, prostaglandin E2, and nicotinamide) from the growth factor cocktail (Figure 1A). This medium, termed "differentiation medium," induced robust stem cell differentiation

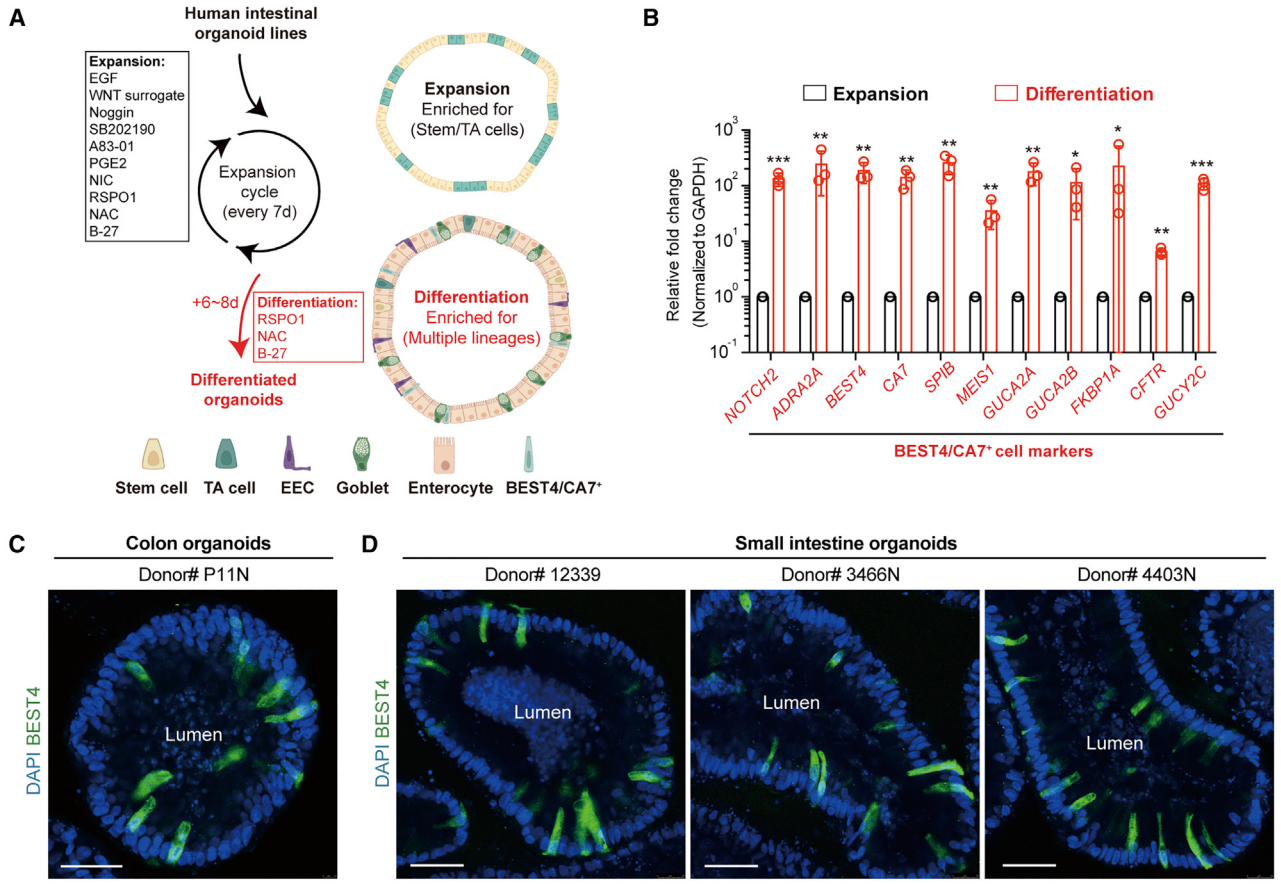

Figure 1. A human intestinal organoid model containing BEST4/CA7$^+$ cells

(A) Schematic of organoid expansion and differentiation. Medium compositions for organoid expansion and differentiation are listed (see also STAR Methods). Representative cell types in the cultured organoids are indicated. EGF, epidermal growth factor; NAC, N-acetyl-L-cysteine; PGE2, prostaglandin E2; NIC, nicotinamide; RSPO1, R-spondin1.

(B) qPCR analysis of a set of BEST4/CA7$^+$ cell markers in colon organoids cultured in expansion or differentiation medium. $n = 3$ biological replicates. Data are presented as mean ± SD. Paired, two-tailed t test is used for comparisons. $^{***}p < 0.001$, $^{**}p < 0.01$, $^{*}p < 0.05$.

(C and D) Representative images of colon (C) and small intestine (D) organoids cultured in differentiation medium. BEST4/CA7$^+$ cells are marked by whole-mount immunofluorescence staining of an antibody against BEST4 (green). Scale bars, 50 μm.

See also Figure S1.

toward multiple cell lineages within 6–8 days (Figure S1A). The expression of a set of intestinal cell-type markers (see below) was compared between expansion and differentiation condition by quantitative polymerase chain reaction (qPCR) analysis (Figure S1A). Efficient induction of the major intestinal cell types was thus achieved, as indicated by the induced expression of enterocyte (marked by *CYP3A4*, *CD36*, and *FABP1*), goblet cell (marked by *MUC2* and *TFF3*), and enteroendocrine cell (EEC, marked by *CHGA* and *TPH1*) markers (Figure S1A). Existence of EECs and goblet cells was further confirmed by whole-mount immunofluorescence staining using a CHGA antibody in reporter organoids in which goblet cells were genetically labeled by a *MUC2-mNeonGreen* knockin allele[15] (Figures S1B and S1C). As expected, we observed reduced expression of stem cell (marked by *LGR5* and *OLFM4*) and TA cell (marked by *MKI67* and *PCNA*) marker genes after removal of the self-renewal factor cocktail (Figure S1A). Expression of *POU2F3* and *AVIL*—marker genes for tuft cells, a rare intestinal epithelial cell type—was not induced in our organoid model owing to the absence of interleukin-4/13 (IL-4/-13), key factors for tuft cell formation[16] (Figure S1A).

By integrating and re-analyzing several published scRNA-seq datasets,[2,17–19] we defined a core set of BEST4/CA7$^+$ cell markers (i.e., *BEST4*, *CA7*, and *SPIB*) (Figures S1D and S1E). Induced expression of these BEST4/CA7$^+$ cell markers was detected by qPCR analysis, implying the existence of this rare cell type in the differentiated organoids (Figure 1B). Immunofluorescence staining using a BEST4 antibody confirmed the presence of BEST4/CA7$^+$ cells in both colon and small intestine organoids derived from multiple unrelated donors (Figures 1C and 1D).

Generation of BEST4/CA7$^+$ cell reporter organoids

For better visualization and further study of BEST4/CA7$^+$ cells, we generated reporter organoids by knocking in a *P2A-tdTomato* cassette at the C terminus of the *CA7* gene (Figures 2A and S1F), using a CRISPR-assisted non-homologous end joining (NHEJ) approach.[20,21] Successful knockin at the *CA7* locus was

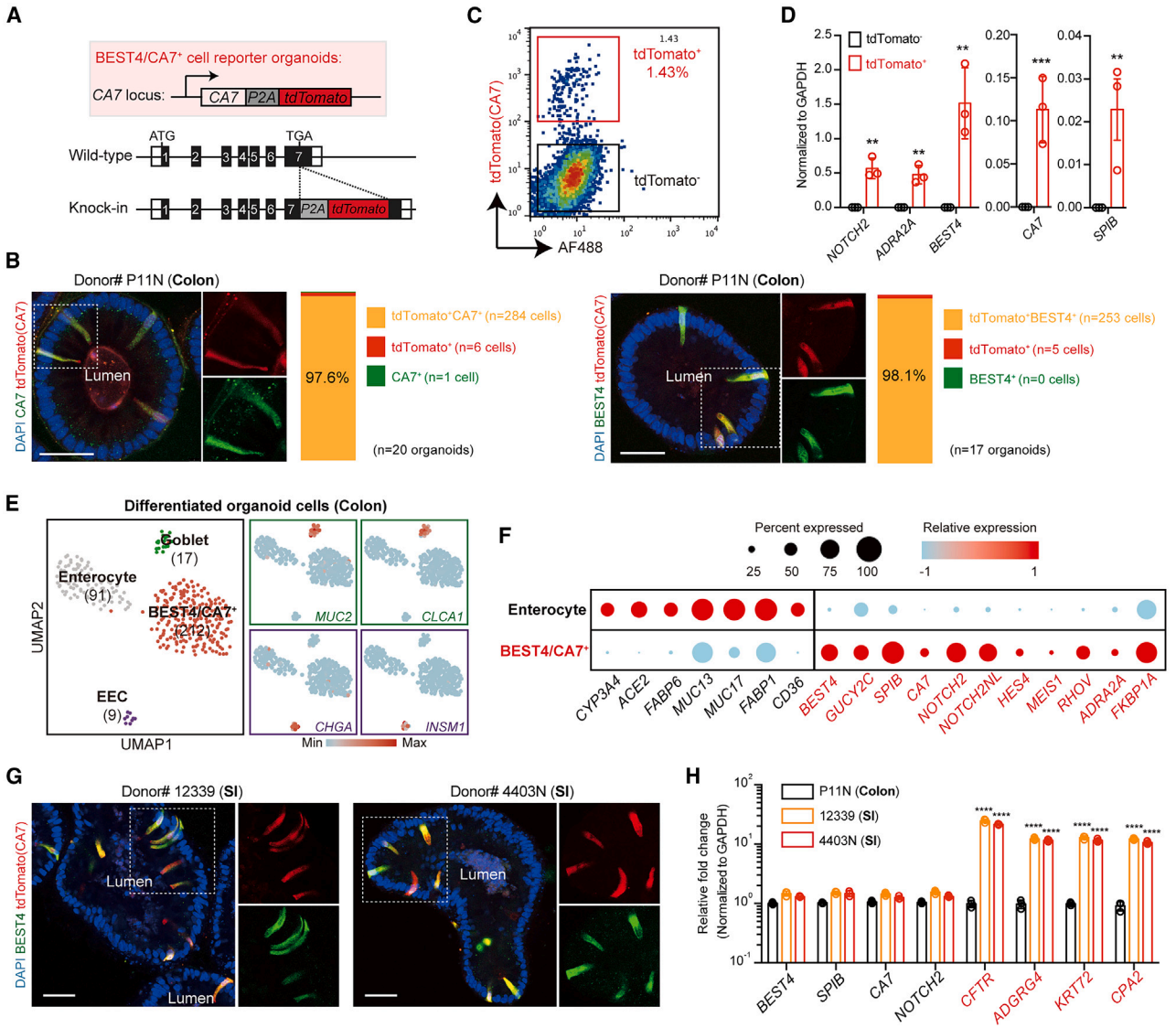

Figure 2. Characterization of BEST4/CA7$^+$ cells using knockin reporter organoids

(A) Illustration of the knockin reporter organoids containing a *P2A-tdTomato* cassette inserted at the C terminus, before the stop codon, of the *CA7* gene.

(B) Representative images of *CA7-P2A-tdTomato* reporter organoids cultured in differentiation medium. Whole-mount immunofluorescence staining with antibodies against CA7 or BEST4 confirms faithful reporter activity in labeling BEST4/CA7$^+$ cells. Scale bars, 50 μm. The percentage of overlap between tdTomato fluorescence and antibody staining signals is shown.

(C) Representative FACS analysis of BEST4/CA7$^+$ cell percentage in *CA7-P2A-tdTomato* reporter organoids cultured in differentiation medium.

(D) qPCR analysis of BEST4/CA7$^+$ cell markers (*NOTCH2*, *ADRA2A*, *BEST4*, *CA7*, and *SPIB*) in sorted tdTomato$^+$ and tdTomato$^-$ cells. $n = 3$ biological replicates. Data are presented as mean ± SD. Paired, two-tailed t test is used for comparisons. $^{***}p < 0.001$, $^{**}p < 0.01$.

(E) scRNA-seq analysis of 329 cells derived from the colon organoids grown in differentiation medium. (Left) Cell clusters are visualized in a uniform manifold approximation and projection (UMAP) plot and colored by different intestinal cell types. Cell numbers are shown in brackets under each indicated cell type. To enrich the BEST4/CA7$^+$ cells for sequencing, tdTomato$^+$ and tdTomato$^-$ cells are sorted from differentiated reporter organoids in 3:1 ratio in cell numbers (see also STAR Methods). (Right) Expression levels and distributions of EEC and goblet cell markers are shown in UMAP plots. The colors, ranging from blue to red, indicate low to high relative gene expression levels.

(F) Dot plot showing the expression of a set of markers for enterocytes and BEST4/CA7$^+$ cells. The color encodes the scaled average expression level across all cells within a cell cluster, and the size of dot encodes the percentage of cells within a class.

(G) Representative images of *CA7-P2A-tdTomato* reporter organoids cultured in differentiation medium and co-stained with a BEST4 antibody. $n = 2$ small intestine (SI) organoid lines are shown. Scale bars, 50 μm.

(H) qPCR analysis of a set of BEST4/CA7$^+$ cell markers in FACS-sorted tdTomato$^+$ cells from *CA7-P2A-tdTomato* reporter organoids derived from colon and SI. For each organoid line, $n = 3$ biological replicates. Data are presented as mean ± SD. One-way ANOVA with Dunnett's test is used for multiple comparisons to the P11N (Colon) group. $^{****}p < 0.0001$.

See also Figure S1.

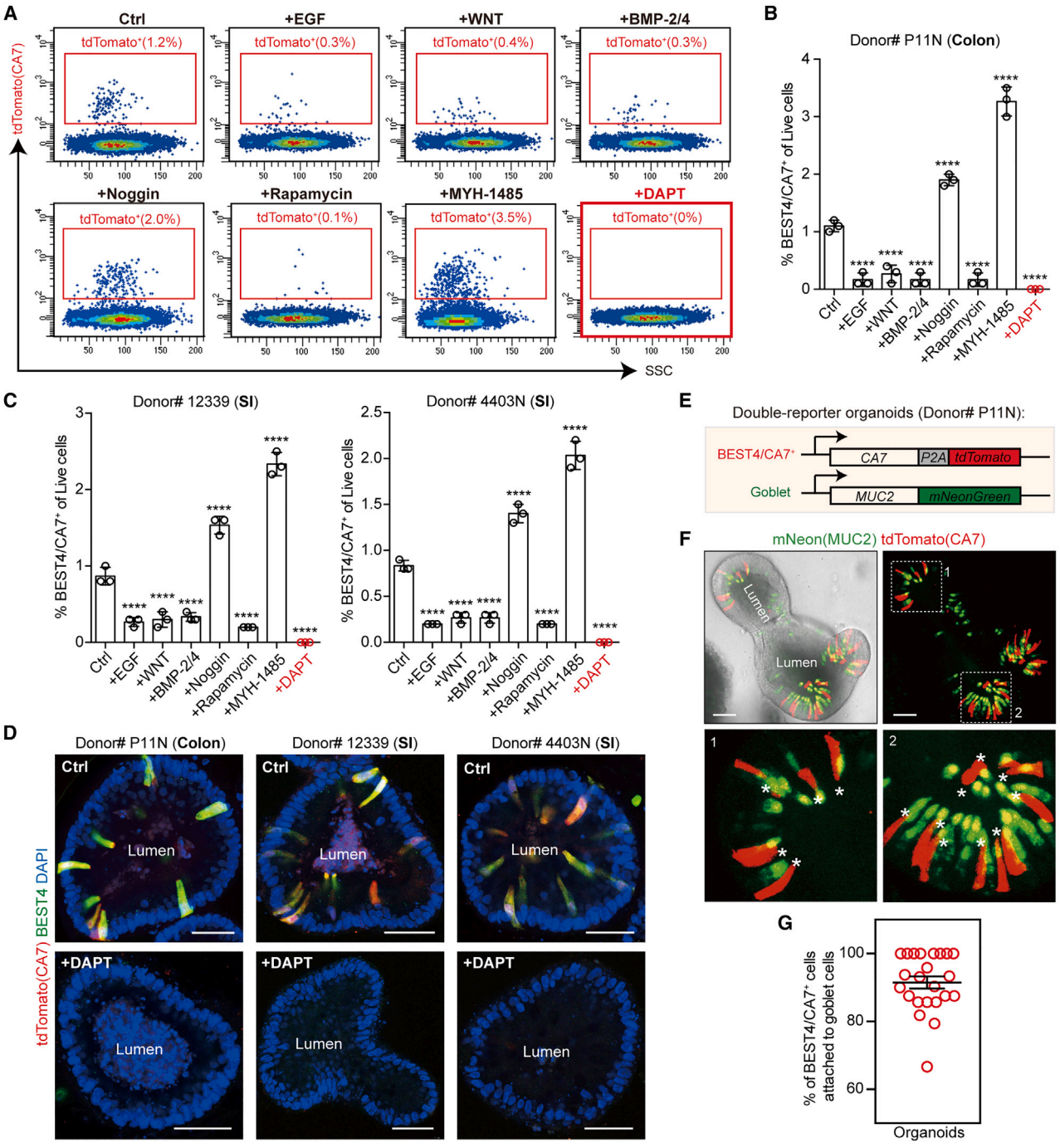

Figure 3. Notch dependency for BEST4/CA7$^+$ cell differentiation

(A–C) Representative FACS analysis (A) and quantification of BEST4/CA7$^+$ cells (B and C) in *CA7-P2A-tdTomato* reporter organoids cultured in differentiation medium (Ctrl) or after adding different niche factors during differentiation. $n = 3$ reporter organoid lines derived from colon and small intestine (SI) are used. FACS quantitation in this study is based on the percentage of reporter fluorescence$^+$ cells among the total DAPI$^-$ live cells (see also STAR Methods). For each factor, $n = 3$ biological replicates. Data are presented as mean ± SD. One-way ANOVA with Dunnett's test is used for multiple comparisons to the Ctrl group. ****$p < 0.0001$. (D) Representative images of *CA7-P2A-tdTomato* reporter organoids cultured in differentiation medium (Ctrl) or after adding DAPT during differentiation. BEST4/CA7$^+$ cells are labeled by tdTomato fluorescence and immunofluorescence staining with an antibody against BEST4 (green). Scale bars, 50 μm. $n = 3$ reporter organoid lines derived from colon and SI are shown.

(legend continued on next page)

validated by targeted genotyping (Figures S1F and S1G; see also STAR Methods), and correct labeling of BEST4/CA7$^+$ cells was confirmed by whole-mount immunofluorescence staining using both CA7 and BEST4 antibodies (Figure 2B). Fluorescence-activated cell sorting (FACS) revealed the presence of approximately 1% tdTomato$^+$ cells in the differentiated organoids (Figure 2C). These tdTomato$^+$ cells expressed multiple BEST4/CA7$^+$ cell markers as demonstrated by FACS sorting followed by qPCR analysis (Figure 2D). Then, BEST4/CA7$^+$ cells (tdTomato$^+$) were enriched by FACS sorting for scRNA-seq analysis, as were BEST4/CA7$^-$ (tdTomato$^-$) cells. After filtering out low-quality cells (Figure S1H), four major cell clusters (representing enterocytes, EECs, goblet cells, and BEST4/CA7$^+$ cells) were identified and annotated based on their signature genes (Figures 2E, 2F, and S1I). BEST4/CA7$^+$ cells expressed a set of markers consistent with published scRNA-seq datasets generated from primary human intestine (Figure 2F, compared with Figure S1E), and they could be readily distinguished from the enterocytes (Figure 2F).

Notably, small-intestinal BEST4/CA7$^+$ cells specifically express *ADGRG4*, *KRT72*, *CPA2*, and *CFTR* (Figure S1E). *CFTR* encodes a Cl^-/HCO_3^- channel and is mutated in cystic fibrosis (CF) patients.[7,22] Of importance to this study, we next generated BEST4/CA7$^+$ cell reporter organoids (*CA7-P2A-tdTomato*) from two small intestine organoid lines. Correct labeling of BEST4/CA7$^+$ cells in the reporter lines was also validated by both immunofluorescence staining using BEST4 antibody (Figure 2G) and qPCR analysis of the BEST4/CA7$^+$ cell markers in FACS-sorted CA7-tdTomato$^+$ cells (Figure S1J). Next, BEST4/CA7$^+$ cells (tdTomato$^+$) were FACS sorted from the colon and small intestine organoids, respectively, and their marker gene expression was compared by qPCR analysis (Figure 2H). BEST4/CA7$^+$ cells derived from small intestine organoids expressed higher levels of *CFTR*, *ADGRG4*, *KRT72*, and *CPA2* (Figure 2H). We concluded that differentiated intestinal organoids contain genuine BEST4/CA7$^+$ cells.

Notch signaling is essential for BEST4/CA7$^+$ cell differentiation

Homeostasis of gut epithelium is maintained by cooperation of multiple niche signals.[23] Using reporter organoids, the effects of these signaling pathways on BEST4/CA7$^+$ cell generation were evaluated and quantified by FACS analysis. Factors representing different niche signals were added to the culture medium during differentiation. Addition of surrogate WNT protein, an essential factor for organoid expansion, strongly inhibited BEST4/CA7$^+$ cell differentiation (Figures 3A and 3B). Similarly, the γ-secretase inhibitor DAPT completely blocked BEST4/CA7$^+$ cell differentiation, indicating an essential role of Notch signaling for BEST4/CA7$^+$ cell generation (Figures 3A and 3B). This agreed with the notion that BEST4/CA7$^+$ cells are closely related to enterocytes, as the latter are also uniquely dependent on Notch signaling.[24] Indeed, a trajectory analysis based on scRNA-seq data predicted BEST4/CA7$^+$ cells to originate from the absorptive lineage.[6] These results were confirmed in two small intestine organoid lines from unrelated donors (Figures 3C and 3D). Activation of Notch signaling requires direct cell-to-cell communication between neighboring cells.[25] BEST4/CA7$^+$ cells highly express the Notch signaling receptor *NOTCH2* (Figures 2D, 2F, S1E, and S1J) and are typically located adjacent to goblet cells *in vivo*.[2,26] Of note, goblet cells express Notch ligands.[24] We observed this unique spatial localization pattern in BEST4/CA7$^+$ and goblet cell double-reporter organoids (Figures 3E–3G). While BEST4/CA7$^+$ cells are closely related to enterocytes, bone morphogenetic protein-2/4 (BMP-2/4), which promotes the maturation of enterocytes,[15] reduced BEST4/CA7$^+$ cell frequency during differentiation. In contrast, noggin, a BMP-inhibitory protein, promoted BEST4/CA7$^+$ cell generation (Figures 3A–3C). Interestingly, BEST4/CA7$^+$ cells express high levels of *FKBP1A* (FK506-binding protein, also known as *FKBP12*) (Figures 2F and S1E). FKBP1A functions as the endogenous rapamycin-binding protein that mediates inhibition of mammalian target of rapamycin (mTOR) signaling.[27,28] The addition of rapamycin strongly inhibited BEST4/CA7$^+$ cell differentiation, suggesting a potential pharmacological strategy for the endogenous control of BEST4/CA7$^+$ cell pool. Activation of mTOR by MHY-1485 increased the numbers of BEST4/CA7$^+$ cells in differentiated organoids (Figures 3A–3C).

Absence of BEST4/CA7$^+$ cells in *SPIB* knockout organoids

BEST4/CA7$^+$ cells derived from primary tissue specifically express the transcription factor (TF) *SPIB* (Figure S1E), and *SPIB* is also expressed by the organoid BEST4/CA7$^+$ cells (Figures 2D, 2F, and S1J). To evaluate its role in cell fate determination, *SPIB* knockout (*SPIB*-KO) organoids were generated using CRISPR[29] (see STAR Methods for details). KO of *SPIB* resulted in complete loss of BEST4/CA7$^+$ cells in the organoids (Figures 4A–4C). We excluded the possibility of CRISPR off-target effect by introducing a doxycycline (Dox)-inducible *SPIB*-overexpression (*SPIB*-OE) construct into these *SPIB*-KO organoids, which specifically rescued the phenotype of BEST4/CA7$^+$ cell loss (Figures 4D and 4E). Whole-mount immunofluorescence staining with the BEST4 antibody (Figure 4F) and qPCR analysis of expression of multiple BEST4/CA7$^+$ cell markers (Figure 4G) further confirmed the loss of the BEST4/CA7$^+$ cell population in these *SPIB*-KO organoids, rather than simply the loss of the CA7 (tdTomato) marker. The *SPIB*-KO effect on BEST4/CA7$^+$ cell generation was then validated in the small intestine organoids derived from a second donor (Figures 4H and 4I).

qPCR analysis showed that expression of the marker genes of SPIB$^-$ cell lineages (including enterocytes, goblet cells, and EECs) was not affected by the loss of *SPIB* (Figure 4J). It has previously been reported that *SPIB* is functionally required for mouse tuft and microfold (M) cells.[30–32] Both cell types, however, are absent in the wild-type (WT) organoids grown in differentiation medium, which lacks the key factors for tuft or M cell

(E and F) Schematic (E) and representative images (F) of *CA7-P2A-tdTomato*; *MUC2-mNeonGreen* double-reporter organoids cultured in differentiation medium. Goblet cells and BEST4/CA7$^+$ cells are marked by mNeonGreen (mNeon) and tdTomato fluorescence, respectively. Asterisks mark BEST4/CA7$^+$ cells that are in proximity to goblet cells. Scale bars, 50 μm.

(G) Proportions of goblet cell-attached BEST4/CA7$^+$ cells in BEST4/CA7$^+$ cell population. $n = 23$ organoids are quantified. Each dot represents one organoid. Data are presented as mean ± SEM.

CellPress
OPEN ACCESS

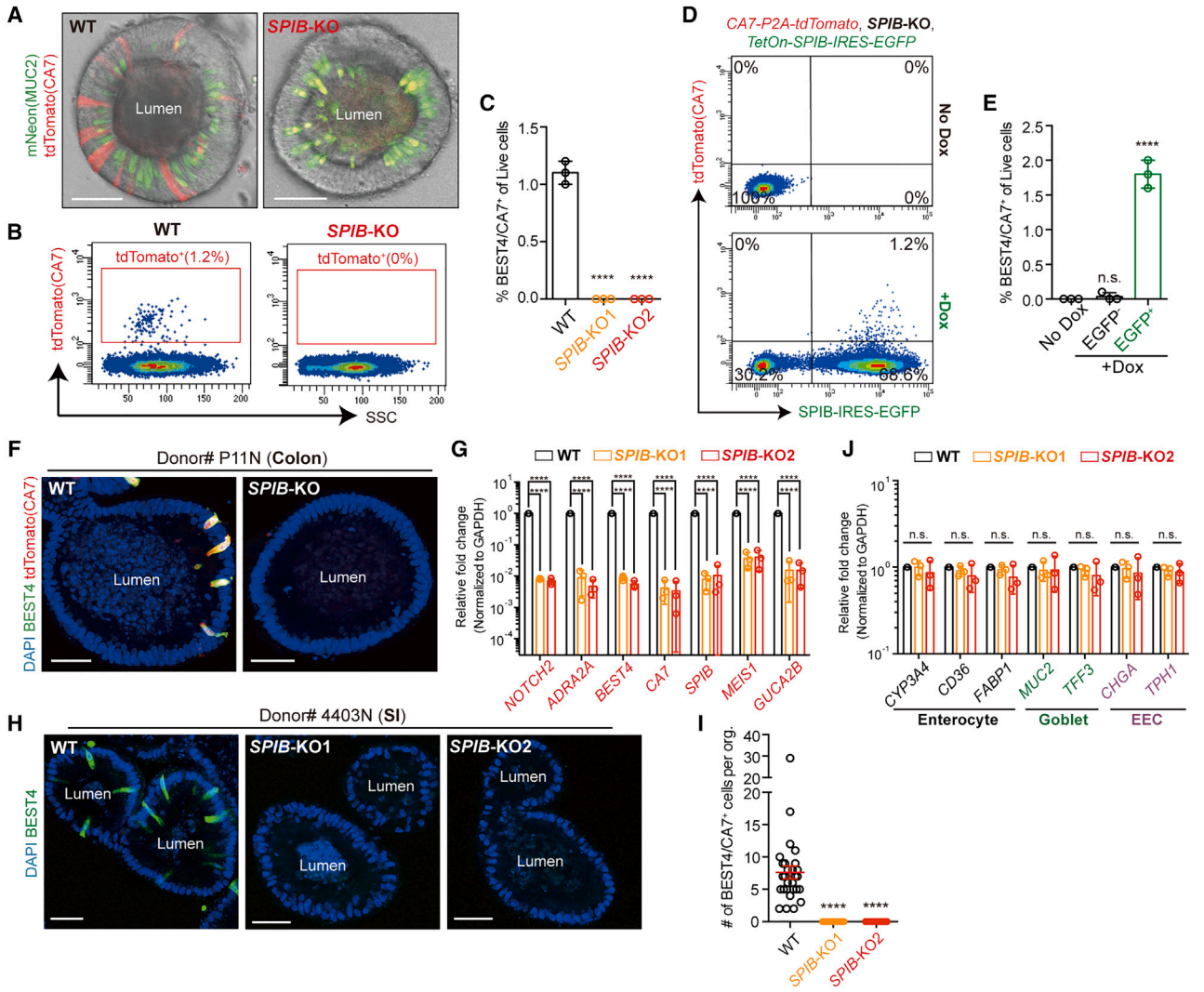

Figure 4. Absence of BEST4/CA7$^+$ cells in *SPIB* knockout organoids

(A) Representative images of differentiated *CA7-P2A-tdTomato*; *MUC2-mNeonGreen* double-reporter organoids with *SPIB*-KO. A wild-type (WT) organoid is shown for comparison. Goblet cells and BEST4/CA7$^+$ cells are marked by mNeonGreen (mNeon) and tdTomato fluorescence, respectively. Scale bars, 50 μm.

(B and C) Representative FACS analysis (B) and quantification of BEST4/CA7$^+$ cells (C) in differentiated WT or *SPIB*-KO double-reporter organoids. BEST4/CA7$^+$ cells are marked by tdTomato fluorescence. $n = 2$ different KO organoid lines are generated. For each *SPIB*-KO organoid line, $n = 3$ biological replicates. Data are presented as mean ± SD. One-way ANOVA with Dunnett's test is used for multiple comparisons to the WT group. ****$p < 0.0001$.

(D and E) Representative FACS analysis (D) and quantification of BEST4/CA7$^+$ cells (E) in differentiated *SPIB*-KO reporter organoids, w/wo Dox-induced *SPIB* overexpression. BEST4/CA7$^+$ cells are marked by tdTomato fluorescence, and *SPIB*-overexpressing cells are marked by EGFP fluorescence. $n = 3$ biological replicates. Data are presented as mean ± SD. One-way ANOVA with Dunnett's test is used for multiple comparisons to the no Dox group. ****$p < 0.0001$; n.s., no significance.

(F) Representative images of differentiated *CA7-P2A-tdTomato* reporter organoids with *SPIB*-KO. A WT organoid is shown for comparison. BEST4/CA7$^+$ cells are marked by tdTomato fluorescence and immunofluorescence staining with an antibody against BEST4 (green). Scale bars, 50 μm.

(G) qPCR analysis of BEST4/CA7$^+$ cell markers in differentiated WT or *SPIB*-KO organoids. $n = 3$ biological replicates. Data are presented as mean ± SD. One-way ANOVA with Dunnett's test is used for multiple comparisons to the WT group. ****$p < 0.0001$.

(H and I) Representative images (H) and quantification of BEST4/CA7$^+$ cell numbers (I) in differentiated WT or *SPIB*-KO small intestine (SI) organoids. BEST4/CA7$^+$ cells are labeled by whole-mount immunofluorescence staining with an antibody against BEST4 (green). Scale bars, 50 μm. $n = 2$ different KO organoid lines are generated. $n = 28$ (in WT group) or 20 (in *SPIB*-KO groups) organoids are quantified. Each dot represents one organoid. Data are presented as mean ± SEM. One-way ANOVA with Dunnett's test is used for multiple comparisons to the WT group. ****$p < 0.0001$.

(J) qPCR analysis of a set of intestinal cell-type markers in differentiated WT or *SPIB*-KO organoids. $n = 3$ biological replicates. Data are presented as mean ± SD. One-way ANOVA with Dunnett's test is used for multiple comparisons to the WT group. n.s., no significance.

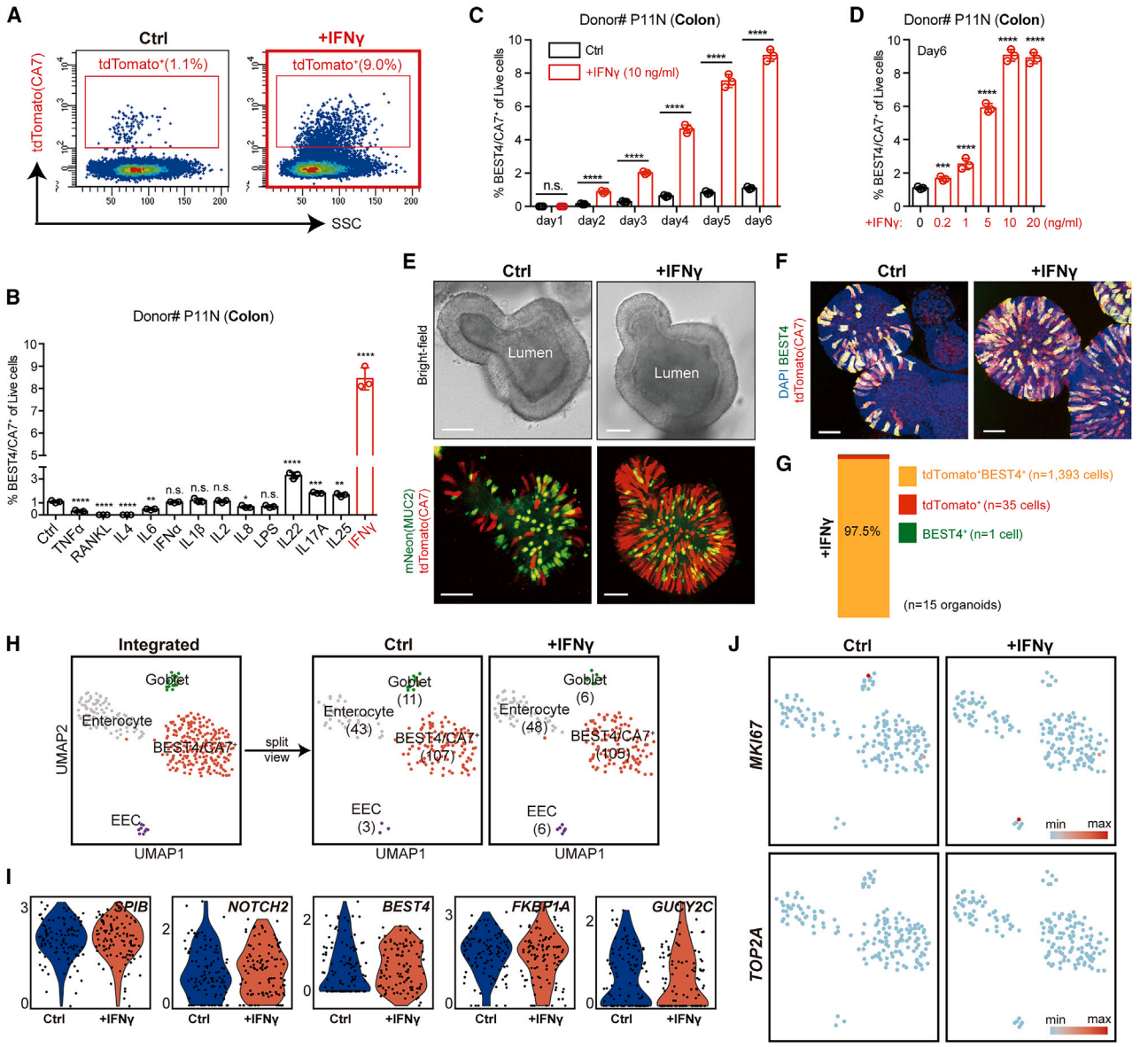

Figure 5. BEST4/CA7$^+$ cell amplification in response to type 1 immune factor IFN-γ

(A) Representative FACS analysis of BEST4/CA7$^+$ cells in *CA7-P2A-tdTomato* reporter organoids cultured in differentiation medium (referred to as the "Ctrl" condition) or after adding IFN-γ during differentiation.

(B) FACS quantification of BEST4/CA7$^+$ cells in *CA7-P2A-tdTomato* reporter organoids cultured in differentiation medium (Ctrl) or after adding different inflammatory factors during differentiation. For each factor, $n = 3$ biological replicates. Data are presented as mean ± SD. One-way ANOVA with Dunnett's test is used for multiple comparisons to the Ctrl group. $^{****}p < 0.0001$, $^{***}p < 0.001$, $^{**}p < 0.01$, $^{*}p < 0.05$; n.s., no significance.

(C) FACS quantification of BEST4/CA7$^+$ cells in differentiated *CA7-P2A-tdTomato* reporter organoids cultured for different days w/wo IFN-γ treatment. $n = 3$ biological replicates for each time point. Data are presented as mean ± SD. Unpaired, two-tailed t test is used for comparisons. $^{****}p < 0.0001$.

(D) FACS quantification of BEST4/CA7$^+$ cells in differentiated *CA7-P2A-tdTomato* reporter organoids in response to different doses of IFN-γ. $n = 3$ biological replicates for each dose. Data are presented as mean ± SD. One-way ANOVA with Dunnett's test is used for multiple comparisons to the no IFN-γ group. $^{****}p < 0.0001$, $^{***}p < 0.001$.

(E) Representative images of *CA7-P2A-tdTomato*; *MUC2-mNeonGreen* double-reporter organoids cultured in differentiation medium (Ctrl) or after adding IFN-γ during differentiation (referred to as the "IFN-γ" condition). Goblet cells and BEST4/CA7$^+$ cells are marked by mNeonGreen (mNeon) and tdTomato fluorescence, respectively. Scale bars, 50 μm.

(F and G) Representative images of differentiated *CA7-P2A-tdTomato* reporter organoids cultured in Ctrl or IFN-γ condition (F). BEST4/CA7$^+$ cells are marked by tdTomato fluorescence and immunofluorescence staining with an antibody against BEST4 (green). Scale bars, 50 μm. The percentage of overlap between tdTomato fluorescence and BEST4 antibody staining signals is shown in (G).

(H) scRNA-seq analysis of differentiated organoid cells cultured in Ctrl or IFN-γ condition. Cell clusters are visualized in UMAP plots and colored by different intestinal cell types. The integrated view (left, same as in Figure 2E) and split view (right) are shown. Cell numbers are shown in brackets under each indicated cell

(legend continued on next page)

differentiation: formation of tuft cells requires IL-4/13,[16] while formation of M cells relies on the receptor activator of nuclear factor κ-B ligand (RANKL).[32,33] For the subsequent functional studies on BEST4/CA7$^+$ cells, we analyzed differentiated *SPIB*-KO organoids (specifically lacking BEST4/CA7$^+$ cells) in comparison with differentiated WT organoids (containing BEST4/CA7$^+$ cells).

BEST4/CA7$^+$ cell amplification in response to type 1 immune factor IFN-γ

BEST4/CA7$^+$ cells represent a rare cell population in healthy gut epithelium. Previous studies have shown that tuft cells and M cells, two other *SPIB*-expressing cell types[30–32] (Figure S1E), increase their numbers in response to specific inflammatory signals: tuft cell amplification is induced by type 2 immune factors IL-4/13 during parasitic infections,[16,34–36] while M cell differentiation requires RANKL.[32,33,37] We investigated whether BEST4/CA7$^+$ cell generation was similarly sensitive to inflammatory signals. By screening a set of cytokines in our BEST4/CA7$^+$ cell reporter organoids, we identified the type 1 immune factor interferon-γ (IFN-γ) to strongly increase BEST4/CA7$^+$ cell numbers as visualized in the *CA7* knockin reporter organoids, i.e., by >8-fold (Figures 5A–5E and S2A). The effect of IFN-γ was further confirmed by dose-response and time-course experiments (Figures 5C and 5D). While most of the other tested inflammatory factors only slightly affected BEST4/CA7$^+$ cell generation (with changes of less than 2-fold), we observed that IL-22 also increased BEST4/CA7$^+$ cell numbers, yet to a lesser extent (∼3.3-fold) than IFN-γ. In contrast, tumor necrosis factor alpha (TNF-α) strongly inhibited BEST4/CA7$^+$ cell differentiation (∼3.6-fold) (Figures 5A, 5B, and S2A).

We further focused on the effect of IFN-γ and confirmed our observation by co-staining with a BEST4 antibody to exclude the possibility of IFN-γ-induced *CA7* gene expression (Figures 5F and 5G). The IFN-γ effect was then validated in small intestine organoids derived from three unrelated donors (Figures S2B–S2D). We next analyzed the effect of IFN-γ in reporter organoids, in which EECs were genetically labeled by a *CHGA-IRES-iRFP670* knockin allele,[38] and goblet cells were labeled by a *MUC2-mNeonGreen* knockin allele.[15] No significant changes were observed in the two secretory cell lineages, indicating that IFN-γ-induced cell expansion was specific to the BEST4/CA7$^+$ cell population (Figures S2E–S2G). In addition, the BMP proteins BMP-2/4, Notch signaling inhibitor DAPT, and mTOR signaling inhibitor rapamycin still suppressed BEST4/CA7$^+$ cell differentiation in the presence of IFN-γ (Figure S2H). Notably, IFN-γ-induced BEST4/CA7$^+$ cell expansion remained fully *SPIB* dependent, as it was completely blocked in *SPIB*-KO organoids (Figure S2H).

We noticed that IL-4 and RANKL, reported to induce tuft cells and M cells, respectively,[16,32,33] exhibited strong inhibitory effects on BEST4/CA7$^+$ cell differentiation (Figures 5B, S3A, and S3B). It thus appeared that differentiation toward the three SPIB$^+$ cell types is under the control of specific immune signals.

To further validate these findings, we generated knockin reporter organoids based on *SPIB* expression (Figures S3C and S3D; see also STAR Methods), in which all SPIB$^+$ cell types were labeled and could be individually distinguished by immunostaining of cell-type markers. Consistent with the qPCR results shown in (Figures 1B and S1A), all SPIB$^+$ cells in organoids cultured in differentiation medium were BEST4/CA7$^+$ cells, while AVIL$^+$ tuft cells were absent (Figures S3E and S3F). Addition of IL-4 completely switched the SPIB$^+$ cell lineages from BEST4/CA7$^+$ cells to AVIL$^+$ tuft cells (Figures S3E and S3F). Similarly, adding RANKL resulted in generating over 60% of SPIB$^+$ cells, of which 2% were GP2$^+$ mature M cells (Figure S3G). No BEST4/CA7$^+$ cell could be detected in RANKL-treated organoids (Figure S3H). AVIL$^+$ tuft cells were also absent in these organoids (Figure S3I). We concluded that these SPIB$^+$ GP2$^-$ cells represent immature M cells, as evidenced by the expression of immature M cell markers[33,39,40] such as *CCL23*, *TNFAIP2*, and *SOX8* in this population (Figure S3J). Of note, these results did not support the conclusion from a previous study based on scRNA-seq analysis, in which the differentiation trajectory of BEST4/CA7$^+$ cells would go through an M-like cell state.[5]

Although *SPIB* appeared crucial for BEST4/CA7$^+$ cell generation, its overexpression alone was not sufficient to induce a BEST4/CA7$^+$ cell lineage, as the percentage of BEST4/CA7$^+$ cells increased by only 1.6-fold in *SPIB*-overexpressing cells (Figures 4D and 4E). Therefore, we also examined the cell-type-specific markers for the other two SPIB$^+$ cell lineages in these *SPIB*-overexpressing cells. While the immature M cell marker *CCL23* was strongly upregulated after *SPIB* overexpression, other immature M cell markers, such as *SOX8* and *TNFAIP2*, as well as the mature M cell marker *GP2*, remained unchanged (Figure S3K). This indicated that *SPIB* overexpression was also not sufficient to induce M cell differentiation, even though *CCL23* is a direct target of SPIB. These findings are consistent with a previous study in mice, showing that *Sox8* is another essential TF for the generation of Gp2$^+$ mature M cells, but the expression of *Sox8* is not regulated by Spib.[39] Furthermore, *SPIB* overexpression failed to induce tuft cells, as neither the expression of tuft cell master regulator *POU2F3* nor the tuft cell marker *AVIL* was upregulated (Figure S3K). Thus, while *SPIB* was necessary for the generation of the three *SPIB*-expressing cell types, it was not sufficient on its own and likely requires additional TFs for complete differentiation.

scRNA-seq analysis of IFN-γ-induced BEST4/CA7$^+$ cells

For a comparison at the transcriptome level, tdTomato$^+$ and tdTomato$^-$ organoid cells cultured in differentiation medium +/− IFN-γ were FACS sorted for scRNA-seq analysis. BEST4/CA7$^+$ cells cultured in these two conditions clustered together (Figure 5H), while IFN-γ-induced BEST4/CA7$^+$ cells exhibited similar expression levels of BEST4/CA7$^+$ cell markers, compared with

type. BEST4/CA7$^+$ (tdTomato$^+$) and BEST4/CA7$^-$ (tdTomato$^-$) cells in Ctrl or IFN-γ condition are enriched in 3:1 ratio in cell numbers by FACS sorting (see also STAR Methods).

(I) Violin plots showing similar expression levels of BEST4/CA7$^+$ cell markers between Ctrl and IFN-γ-induced BEST4/CA7$^+$ cells.

(J) UMAP plots showing the expression levels and distributions of proliferation markers (*MKI67* and *TOP2A*) in organoid-derived cells grown in Ctrl or IFN-γ condition. The colors, ranging from blue to red, indicate low to high relative gene expression levels.

See also Figures S2–S4.

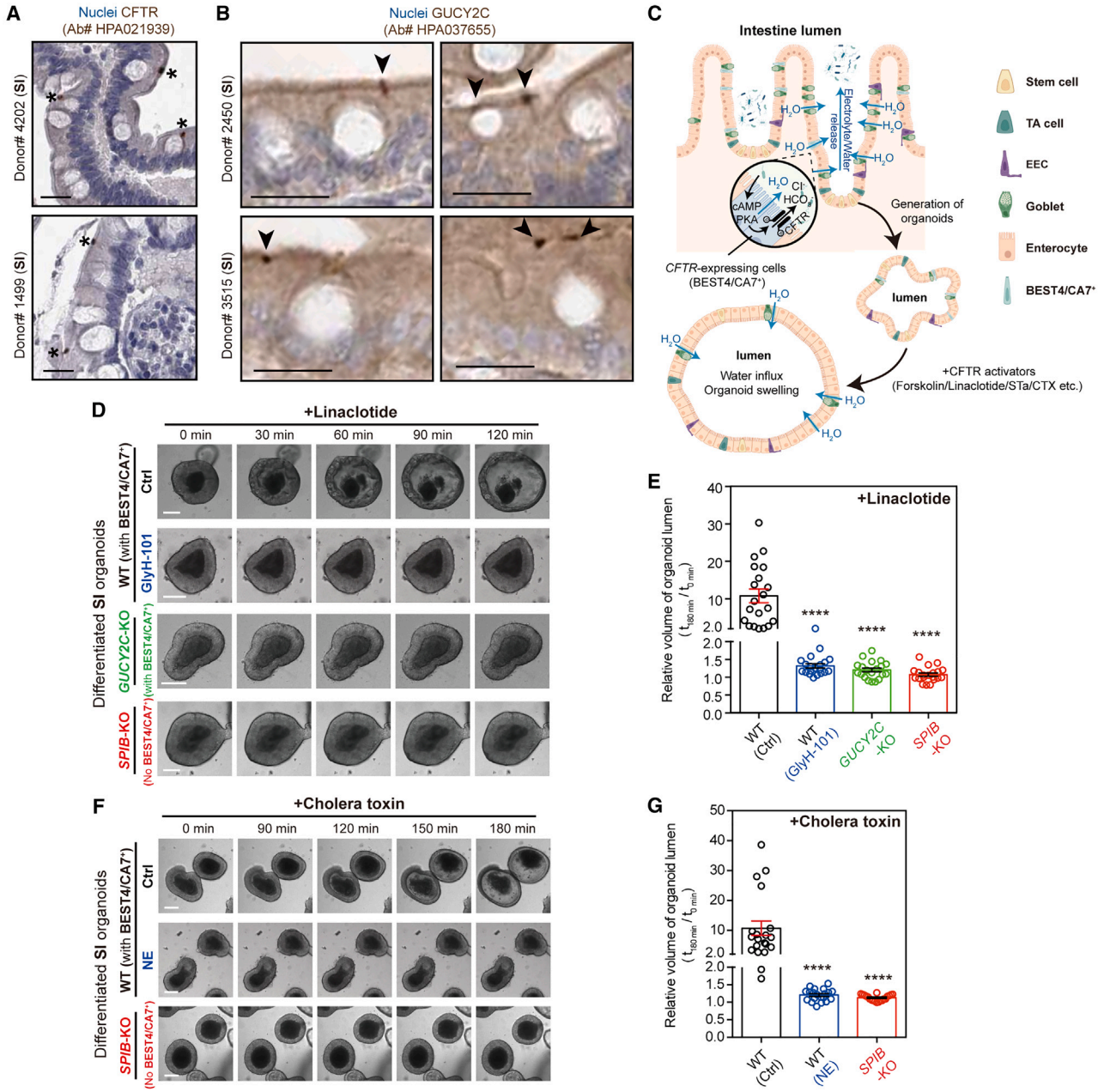

Figure 6. BEST4/CA7⁺ cells control electrolyte/fluid homeostasis

(A and B) Immunohistochemistry (IHC) staining with antibodies directed against CFTR (A) or GUCY2C (B) on the human small intestine (SI) sections. Positive staining signals of CFTR (marked by the asterisks) or GUCY2C (marked by the arrowheads) are detected on the apical surface of BEST4/CA7⁺ cells near the goblet cells. Images are derived from the Human Protein Atlas (https://www.proteinatlas.org/). Scale bars, 20 μm.

(C) Schematic of modeling bacterial diarrheal toxin-induced fluid secretion with organoid swelling assay. Bacterial infections activate intracellular cyclic adenosine monophosphate (cAMP)-protein kinase A (PKA) signaling, leading to CFTR phosphorylation and electrolyte release. Imbalanced ion levels between the basal and apical side of the gut epithelium result in water efflux into the gut lumen. Similarly, in the intestinal organoid model, activation of CFTR causes water influx into the organoid lumen, resulting in organoid swelling.

(D and E) Representative time-lapse images (D) and quantification of the relative changes in organoid lumen volume (E) in response to the STa analog linaclotide. WT (treated w/wo CFTR inhibitor GlyH-101), *SPIB*-KO, and *GUCY2C*-KO SI organoids cultured in differentiation medium are analyzed. Scale bars, 100 μm. $n = 20$ organoids are measured for each group. Each dot represents one organoid. For each organoid, the lumen volume at t = 180 min is normalized to the lumen volume at t = 0 min (set as 1.0). $n = 2$ different SI donors are used to validate the GlyH-101 effect. $n = 2$ *SPIB*-KO or *GUCY2C*-KO clonal organoid lines generated from one SI donor are tested. Data are presented as mean ± SEM. One-way ANOVA with Dunnett's test is used for multiple comparisons to the WT (Ctrl) group. ****$p < 0.0001$.

(F and G) Representative time-lapse images (F) and quantification of the relative changes in organoid lumen volume (G) in response to cholera toxin. WT (treated w/wo norepinephrine, NE) and *SPIB*-KO SI organoids cultured in differentiation medium are analyzed. Scale bars, 100 μm. $n = 20$ organoids are measured for

(legend continued on next page)

the IFN-γ-naive BEST4/CA7$^+$ cells (Figure 5I). When primary scRNA-seq datasets were included, organoid BEST4/CA7$^+$ cells cultured in both conditions clustered with the primary BEST4/CA7$^+$ cell population, with comparable marker gene expression (Figures S4A and S4B), further confirming their cellular identity. Of note, IFN-γ-induced BEST4/CA7$^+$ cell expansion appeared to derive by *de novo* generation from stem/TA cells rather than by self-duplication of pre-existing mature BEST4/CA7$^+$ cells, as no proliferation markers were detected in IFN-γ-induced BEST4/CA7$^+$ cells (Figure 5J).

We next performed live-cell tracking in the reporter organoids (+/− IFN-γ) to document how BEST4/CA7$^+$ cells are generated in the presence of IFN-γ. Similar to the control condition (without IFN-γ treatment), the generation of IFN-γ-induced BEST4/CA7$^+$ cells occurred directly from undifferentiated cells (CA7-tdTomato$^-$), rather than through the duplication of pre-existing CA7-tdTomato$^+$ cells (Figure S4C, top and middle). These IFN-γ-induced BEST4/CA7$^+$ cells did not proliferate to generate tdTomato$^+$ progeny during the 24-h tracing period after their formation (Figure S4C, bottom). These lineage tracing results aligned with our observations from the scRNA-seq analysis. Furthermore, we conducted a nucleotide pulse-chase experiment by labeling stem/TA cells with bromodeoxyuridine (BrdU) during the expansion stage and using EdU to capture BEST4/CA7$^+$ cell formation during differentiation, with or without IFN-γ treatment (Figure S4D). The generated BEST4/CA7$^+$ cells were primarily BrdU$^+$, and they did not incorporate EdU, confirming that they were derived from the stem/TA cells rather than through self-duplication (Figure S4D). The scRNA-seq analysis, live-cell tracking, and EdU-labeling experiments all suggested that there are very few proliferating stem/TA cells in our differentiated organoids. Proliferating stem/TA cells indeed can still persist under some conditions that promote cell differentiation.[13,41] However, in these cases, the differentiation media do still contain factors that support stem cell growth, including EGF, WNT, Noggin, and A83-01. In clear contrast, in our optimized BEST4/CA7$^+$ cell differentiation medium, we have to remove WNT and EGF, as they strongly suppress BEST4/CA7$^+$ cell differentiation. Thus, it is fully expected that there are very few stem/TA cells remaining in the organoids that have been cultured in our differentiation medium for 6–8 days.

Notably, it appeared unlikely that IFN-γ promotes *de novo* differentiation toward BEST4/CA7$^+$ cell lineage through a direct induction of *SPIB* expression. Our scRNA-seq data suggested that *SPIB* is not an IFN-γ target gene, as IFN-γ did not induce *SPIB* expression in non-BEST4/CA7$^+$ cell types (i.e., the enterocytes), nor did it induce a higher expression level of *SPIB* in BEST4/CA7$^+$ cells (Figure S4E). Furthermore, the addition of IFN-γ could not induce the expression of BEST4/CA7$^+$ cell markers (such as *BEST4*, *CA7*, and *SPIB*) in organoids cultured in expansion medium (Figure S4F). However, the activity of many TFs can also be regulated by subcellular localization, protein-protein interaction, and/or posttranslational modification. Thus, while *SPIB* mRNA is unaltered by IFN-γ, we cannot exclude that its activity could be modulated in other ways.

We next analyzed the existence of differentially expressed genes (DEGs) in IFN-γ-induced BEST4/CA7$^+$ cells as compared with their IFN-γ-naive counterparts. Only 43 DEGs were found (with a threshold set at 1.5-fold), within which "antigen-presenting-related genes" were enriched (Figures S4G and S4H). These genes are well-known IFN-γ targets in immune cells.[42] Other IFN-γ-induced genes that exhibited increased expression included the oligoadenylate synthetases (OAS) proteins[42] and tripartite motif-containing (TRIM) family proteins[43] (Figure S4H). Most DEGs could be detected in a small proportion of primary tissue-derived BEST4/CA7$^+$ cells (Figure S4I). We then compared the expression of these IFN-γ-induced genes in BEST4/CA7$^+$ cells derived from individual non-diseased primary intestinal tissues.[2] Based on the percentages of BEST4/CA7$^+$ cells within total epithelial cells (Figure S4J, ranging from 0.5% to 22.9%), these primary tissues could be divided into high BEST4/CA7$^+$ groups (5.1% to 22.9%, comparable to the percentages of IFN-γ-treated organoids, which range from 6.4% to 8.4%) and low BEST4/CA7$^+$ groups (0.5% to 3.1%, comparable to the percentages of IFN-γ-naive organoids, which range from 0.8% to 1.3%). BEST4/CA7$^+$ cells derived from the high BEST4/CA7$^+$ groups exhibited higher expression levels of IFN-γ-induced genes (Figure S4K), suggesting that IFN-γ-induction of BEST4/CA7$^+$ cell expansion also occurs *in vivo*.

BEST4/CA7$^+$ cells are cellular targets of bacterial diarrheal toxins

Unlike mouse intestinal epithelium, which broadly expresses *Cftr*,[44–46] BEST4/CA7$^+$ cells are the only *CFTR*-high expressers in human small intestine (Figures 2H and S1E). Pathological conditions such as bacterial infections can cause an imbalance in fluid homeostasis by targeting CFTR through a diversity of mechanisms[11,47,48] (Figure S5A). Enterotoxigenic *Escherichia coli* (ETEC) infection causes bacterial diarrheal illness by producing heat-stable enterotoxin (STa), which targets GUCY2C,[49,50] a transmembrane receptor encoding the enzyme guanylate cyclase C (GC-C). An activating *GUCY2C* mutation has been identified in familial diarrhea syndrome.[51] STa binding and the subsequent activation of GUCY2C lead to CFTR phosphorylation[49,52] (Figure S5A). In human small intestine, only BEST4/CA7$^+$ cells and EECs express high levels of *GUCY2C* (Figure S1E). A recent study has shown that EECs are *GUCY2C*-high expressers and has proposed a role of GUCY2C signaling in regulating visceral pain.[53] Of note, EECs do not express *CFTR* (Figure S1E). We confirmed that *GUCY2C* expression is restricted to human BEST4/CA7$^+$ cells and EECs (Figure S5B). At the protein level and similar to CFTR, GUCY2C is highly concentrated on the apical surface of BEST4/CA7$^+$ cells (Figures 6A, 6B, S5C, and S5D), suggesting that STa could function through these GUCY2C-expressing BEST4/CA7$^+$ cells (Figure S5A). Although *GUCY2C* is highly expressed by BEST4/CA7$^+$ cells, it is not a direct target of the SPIB, as *SPIB* overexpression failed to upregulate *GUCY2C* expression (Figure S5E).

each group. Each dot represents one organoid. For each organoid, the lumen volume at t = 180 min is normalized to the lumen volume at t = 0 min (set as 1.0). $n = 2$ different SI donors are used to validate the NE effect. $n = 2$ *SPIB*-KO clonal organoid lines generated from one SI donor are tested. Data are presented as mean ± SEM. One-way ANOVA with Dunnett's test is used for multiple comparisons to the WT (Ctrl) group. ****$p < 0.0001$.
See also Figure S5.

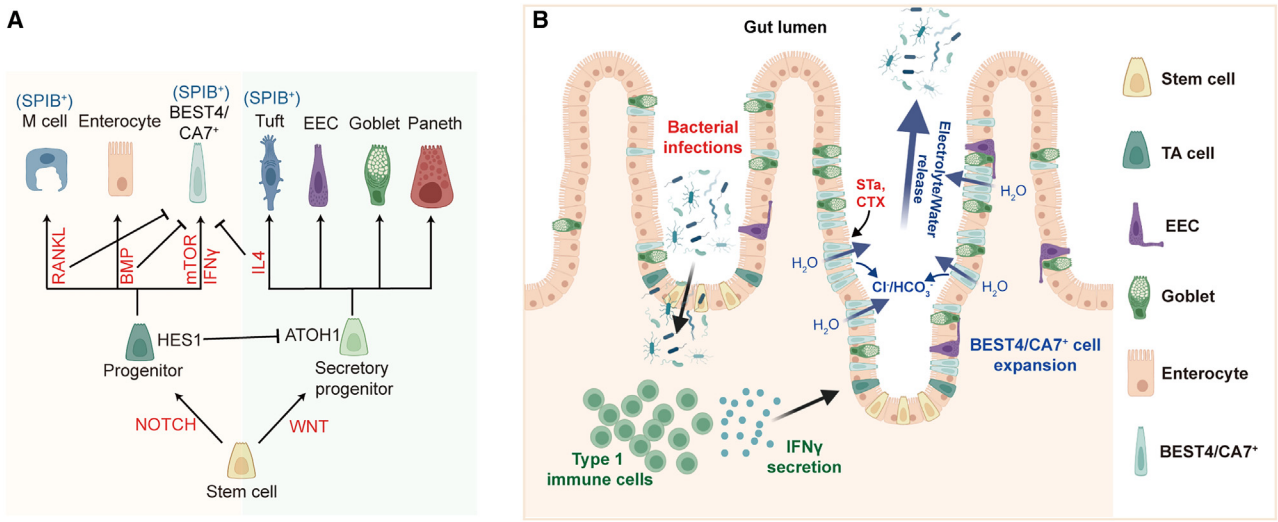

Figure 7. Schematic of BEST4/CA7$^+$ cell differentiation and function

(A) Summary of BEST4/CA7$^+$ cell differentiation. Niche signals and inflammatory factors identified to promote or inhibit BEST4/CA7$^+$ cell differentiation are labeled in red.

(B) Model of bacterial diarrheal toxin-induced imbalance in fluid homeostasis mediated by BEST4/CA7$^+$ cells. Bacterial infections expand the BEST4/CA7$^+$ cell pool by stimulating type 1 immune cells to release IFN-γ, which amplifies electrolyte/water release induced by bacterial toxins upon activation of CFTR on these IFN-γ-induced BEST4/CA7$^+$ cells.

We have shown previously that induced fluid efflux mediated through CFTR activation can be recapitulated in organoid models.[54] A CFTR activator, such as forskolin, could induce fluid influx into organoid lumen, leading to organoid swelling (Figure 6C). This organoid-based assay has been extensively used in CF research and, for instance, for personalized CF patient treatment.[54,55] We tested BEST4/CA7$^+$ cell function in STa-induced imbalance in fluid homeostasis by performing swelling assays on small intestine organoids stimulated with the STa analog linaclotide[56,57] (Figures 6D and 6E). Linaclotide triggered robust water influx and organoid swelling in differentiated organoids containing BEST4/CA7$^+$ cells (Figures 6D and 6E). Swelling of organoids was mediated by CFTR activation, as it could be completely blocked by the CFTR-specific inhibitor GlyH-101[58] (Figures 6D and 6E). Of note, long-term blockade of CFTR function by GlyH-101 resulted in a significant decrease in BEST4/CA7$^+$ cell numbers (Figure S5F). Similarly, KO of *BEST4*, another Cl^-/HCO_3^- ion channel,[8] led to a dramatic loss of BEST4/CA7$^+$ cells (Figure S5G). In contrast, KO of *CA7*, the BEST4/CA7$^+$ cell marker that encodes a carbonic anhydrase, had little effect on BEST4/CA7$^+$ cell generation (Figure S5H). In addition, GUCY2C was found to be a dispensable receptor for the generation of BEST4/CA7$^+$ cells (Figure S5I). Yet, its essential role in mediating linaclotide-induced organoid swelling was confirmed in the *GUCY2C*-KO organoids (Figures 6D and 6E).

To test whether the organoid swelling was mediated by BEST4/CA7$^+$ cells, we next assayed the *SPIB*-KO organoids (devoid of BEST4/CA7$^+$ cells) and found that the swelling response was indeed absent in these organoids (Figures 6D and 6E). Since *SPIB*-KO organoids still contain EECs that also express high levels of *GUCY2C*, this result agreed with the notion that EECs are not involved in electrolyte/fluid homeostasis as they do not express *CFTR*. Taken together, our results demonstrate that BEST4/CA7$^+$ cells are the primary targets of STa and thus mediate ETEC-induced imbalance in fluid homeostasis.

Vibrio cholerae (*V. cholerae*) is the etiological agent of cholera and induces rapid and severe dehydration.[48,59] Cholera toxin (CTX), secreted by *V. cholerae*, is the direct cause of profuse, watery diarrhea. Mechanistic studies have found that CTX also open the CFTR channel for anion efflux.[11,59] Similar to STa, CTX efficiently induced swelling of differentiated organoids (Figures 6F and 6G). This process was again mediated by BEST4/CA7$^+$ cells as the swelling response was absent in *SPIB*-KO organoids (Figures 6F and 6G). In addition, the direct response of BEST4/CA7$^+$ cells to CTX was further validated using a genetically encoded cAMP sensor[60] (Figures S5J and S5K). Of note, BEST4/CA7$^+$ cells highly and specifically express *ADRA2A*, the α2A adrenergic receptor (Figures 2D and S5L), which is the only adrenergic receptor family member highly expressed in human intestinal epithelium. α2 adrenergic receptors inhibit cAMP-mediated secretion when stimulated by ligands such as norepinephrine (NE).[61] Addition of NE, to inhibit cAMP signaling through ADRA2A in BEST4/CA7$^+$ cells, strongly blocked CTX-induced organoid swelling (Figures 6F and 6G), implying that ADRA2A signaling could be a potential mechanism for endogenous control of electrolyte/fluid homeostasis in BEST4/CA7$^+$ cells.

DISCUSSION

In this study, we describe culture conditions to generate BEST4/CA7$^+$ cells in human intestinal organoids, which has allowed us to evaluate the effects of different niche signals and TF on BEST4/CA7$^+$ cell differentiation (Figure 7A). Within these tested factors, we identify IFN-γ, a type 1 immune factor, as a specific

amplifier of BEST4/CA7$^+$ cell population. Intestinal tuft cells and goblet cells are known as the type 2 immune-responsive cells during parasitic infections, as they are inducible by the type 2 immune factor IL-4/13.[16,34–36] It was previously unclear whether type 1 immune-responsive cells exist in the gut epithelium. The responsiveness to IFN-γ demonstrates for the first time that BEST4/CA7$^+$ cells serve as a type 1 immune-responsive cell type in human intestine.

IFN-γ production can be stimulated by bacterial infections,[62] which implies that BEST4/CA7$^+$ cells may function in bacterial defense. Watery diarrhea is an effective host response to wash out unwanted bacteria.[11,63] In mouse intestine, a BEST4/CA7$^+$ cell counterpart has not come forward from scRNA-seq analysis.[10] Rather, *Cftr* and *Gucy2c* are broadly expressed in murine gut epithelium.[44–46,53,64] In human intestinal epithelium, BEST4/CA7$^+$ cells appear to be specialized enterocytes, evolved away from the "standard" enterocytes to specifically regulate electrolyte/fluid homeostasis. BEST4/CA7$^+$ cells are the only human intestinal cells that highly express both *CFTR* and *GUCY2C* and thus represent the major cellular targets of STa. It is important to note that bacterial infections of the intestine can induce an imbalance in fluid homeostasis through a variety of mechanisms.[11,48] Similar to the STa-GUCY2C axis, most of these mechanisms will eventually target and activate CFTR. Indeed, we confirm that cholera toxin, derived from diarrhea-causing *V. cholerae*, also induces water efflux by targeting BEST4/CA7$^+$ cells. Notably, several mouse models have previously been used to study Cftr-mediated bacterial diarrhea.[65,66] However, these studies likely focused on stem/TA cells and enterocytes, rather than on BEST4/CA7$^+$ cells. Therefore, applying the findings from mouse models to humans may require further validation using our BEST4/CA7$^+$ cell organoids. Since BEST4/CA7$^+$ cells only represent a small fraction of the intestinal epithelium, our findings propose a model in which bacterial infections expand the BEST4/CA7$^+$ cell pool by stimulating type 1 immune cells to release IFN-γ, which in turn amplifies the electrolyte/water release induced by bacterial toxins upon the activation of CFTR on these IFN-γ-induced BEST4/CA7$^+$ cells (Figure 7B). Taken together, our experimental observations highlight roles of BEST4/CA7$^+$ cells in electrolyte homeostasis, as well as diarrhea in response to bacterial infections.

Limitations of the study

In this study, we investigate the differentiation and function of human BEST4/CA7$^+$ cells using *in vitro* intestinal organoid models, allowing for the assessment of their responses to specific niche factors, cytokines, and bacterial toxins in isolation. While the organoid platform has many experimental advantages over *in vivo* studies, it in essence is a reductionist system that requires translation into more complex *in vivo* settings. This however poses several challenges: (1) mouse models are not suitable since they lack BEST4/CA7$^+$ cells; (2) clinical data from patients with inflammatory bowel disease (IBD) are complicated to interpret because of the involvement of multiple cytokines beyond IFN-γ. For instance, TNF-α, another pro-inflammation cytokine elevated in IBD, strongly inhibits BEST4/CA7$^+$ cell generation in our hands; and (3) how BEST4/CA7$^+$ cells respond to live bacteria requires further study.

RESOURCE AVAILABILITY

Lead contact

Further information and requests for resources and reagents should be directed to and will be fulfilled by the lead contact, Hans Clevers (h.clevers@hubrecht.eu).

Materials availability

Unique and stable reagents generated in this study are available and can be requested from the lead contact. Sharing the organoid lines used in this study requires approval from our local Institutional Review Board. A completed materials transfer agreement will also be required.

Data and code availability

The organoid scRNA-seq dataset generated in this study has been deposited at Gene Expression Omnibus (GEO) under the accession number GEO: GSE242765 and is publicly available. This paper does not report original code.

ACKNOWLEDGMENTS

We thank Reinier van der Linden and Anita Pfauth from Hubrecht FACS Facility for cell sorting. We thank Single-Cell Discovery for technical support in scRNA-seq experiments. We thank Dr. Lanyue Bai from BeiGene for helpful discussion. This work is supported by the Netherlands Organ-on-Chip Initiative, an NWO Gravitation project (no. 024.003.001) funded by the Ministry of Education, Culture and Science of the Government of the Netherlands (to H.C.); the project Organoids in Time with project no. 2019.085 of the research program NWO Investment Large financed by the Dutch Research Council (to H.C., J.S.v.Z., and S.J.T.); and a Marie Skłodowska-Curie grant (no. 10126478) (to D.K.).

AUTHOR CONTRIBUTIONS

D.W. conceptualized the project, designed and performed experiments, interpreted the results, and wrote the manuscript; W.K.S. imaged organoids and W.K.S., J.S.v.Z., and S.J.T. interpreted the imaging results; L.L. provided plasmid constructs and helped to generate the EEC reporter organoids; N.A. provided an sgRNA plasmid used for generating KO organoids; D.K. provided several plasmids for the generation of knockin reporter organoids and helped in organoid imaging; T.D. established several organoid lines used in this study; and J.H.v.E. and H.C. conceptualized and supervised the project and wrote the manuscript.

DECLARATION OF INTERESTS

H.C. is the head of Pharma Research and Early Development at Roche, Basel and holds several patents related to organoid technology. His full disclosure can be found at https://www.uu.nl/staff/JCClevers.

STAR★METHODS

Detailed methods are provided in the online version of this paper and include the following:

- KEY RESOURCES TABLE
- EXPERIMENTAL MODEL AND STUDY PARTICIPANT DETAILS
  - Human intestinal organoid lines
- METHOD DETAILS
  - Organoid culture and differentiation
  - Generation of genetically modified organoids
  - Immuno-staining and confocal imaging
  - Live cell tracking
  - Nucleotide pulse-chase experiment and EdU/BrdU labeling
  - Imaging of cAMP sensor
  - Sample preparation and flow cytometry
  - Sample preparation for scRNA-seq analysis
  - Analysis of organoid scRNA-seq datasets
  - Analysis of primary intestinal scRNA-seq datasets

SUPPLEMENTAL INFORMATION

Supplemental information can be found online at https://doi.org/10.1016/j.stem.2025.02.003.

Received: April 3, 2024
Revised: September 25, 2024
Accepted: February 4, 2025
Published: February 25, 2025

REFERENCES

1. Hickey, J.W., Becker, W.R., Nevins, S.A., Horning, A., Perez, A.E., Zhu, C., Zhu, B., Wei, B., Chiu, R., Chen, D.C., et al. (2023). Organization of the human intestine at single-cell resolution. Nature *619*, 572–584. https://doi.org/10.1038/s41586-023-05915-x.
2. Elmentaite, R., Kumasaka, N., Roberts, K., Fleming, A., Dann, E., King, H.W., Kleshchevnikov, V., Dabrowska, M., Pritchard, S., Bolt, L., et al. (2021). Cells of the human intestinal tract mapped across space and time. Nature *597*, 250–255. https://doi.org/10.1038/s41586-021-03852-1.
3. Busslinger, G.A., Weusten, B.L.A., Bogte, A., Begthel, H., Brosens, L.A.A., and Clevers, H. (2021). Human gastrointestinal epithelia of the esophagus, stomach, and duodenum resolved at single-cell resolution. Cell Rep. *34*, 108819. https://doi.org/10.1016/j.celrep.2021.108819.
4. Burclaff, J., Bliton, R.J., Breau, K.A., Ok, M.T., Gomez-Martinez, I., Ranek, J.S., Bhatt, A.P., Purvis, J.E., Woosley, J.T., and Magness, S.T. (2022). A Proximal-to-Distal Survey of Healthy Adult Human Small Intestine and Colon Epithelium by Single-Cell Transcriptomics. Cell. Mol. Gastroenterol. Hepatol. *13*, 1554–1589. https://doi.org/10.1016/j.jcmgh.2022.02.007.
5. Smillie, C.S., Biton, M., Ordovas-Montanes, J., Sullivan, K.M., Burgin, G., Graham, D.B., Herbst, R.H., Rogel, N., Slyper, M., Waldman, J., et al. (2019). Intra- and Inter-cellular Rewiring of the Human Colon during Ulcerative Colitis. Cell *178*, 714–730.e22. https://doi.org/10.1016/j.cell.2019.06.029.
6. Parikh, K., Antanaviciute, A., Fawkner-Corbett, D., Jagielowicz, M., Aulicino, A., Lagerholm, C., Davis, S., Kinchen, J., Chen, H.H., Alham, N.K., et al. (2019). Colonic epithelial cell diversity in health and inflammatory bowel disease. Nature *567*, 49–55. https://doi.org/10.1038/s41586-019-0992-y.
7. Greger, R. (2000). Role of CFTR in the Colon. Annu. Rev. Physiol. *62*, 467–491. https://doi.org/10.1146/annurev.physiol.62.1.467.
8. Hartzell, H.C., Qu, Z., Yu, K., Xiao, Q., and Chien, L.-T. (2008). Molecular Physiology of Bestrophins: Multifunctional Membrane Proteins Linked to Best Disease and Other Retinopathies. Physiol. Rev. *88*, 639–672. https://doi.org/10.1152/physrev.00022.2007.
9. Tu, Y.-H., Cooper, A.J., Teng, B., Chang, R.B., Artiga, D.J., Turner, H.N., Mulhall, E.M., Ye, W., Smith, A.D., and Liman, E.R. (2018). An evolutionarily conserved gene family encodes proton-selective ion channels. Science *359*, 1047–1050. https://doi.org/10.1126/science.aao3264.
10. Ishikawa, K., Sugimoto, S., Oda, M., Fujii, M., Takahashi, S., Ohta, Y., Takano, A., Ishimaru, K., Matano, M., Yoshida, K., et al. (2022). Identification of Quiescent LGR5+ Stem Cells in the Human Colon. Gastroenterology *163*, 1391–1406.e24. https://doi.org/10.1053/j.gastro.2022.07.081.
11. Viswanathan, V.K., Hodges, K., and Hecht, G. (2009). Enteric infection meets intestinal function: how bacterial pathogens cause diarrhoea. Nat. Rev. Microbiol. *7*, 110–119. https://doi.org/10.1038/nrmicro2053.
12. Sato, T., Stange, D.E., Ferrante, M., Vries, R.G.J., van Es, J.H., van den Brink, S., van Houdt, W.J., Pronk, A., van Gorp, J., Siersema, P.D., et al. (2011). Long-term Expansion of Epithelial Organoids From Human Colon, Adenoma, Adenocarcinoma, and Barrett's Epithelium. Gastroenterology *141*, 1762–1772. https://doi.org/10.1053/j.gastro.2011.07.050.
13. He, G.-W., Lin, L., DeMartino, J., Zheng, X., Staliarova, N., Dayton, T., Begthel, H., van de Wetering, W.J., Bodewes, E., van Zon, J., et al. (2022). Optimized human intestinal organoid model reveals interleukin-22-dependency of paneth cell formation. Cell Stem Cell *29*, 1333–1345.e6. https://doi.org/10.1016/j.stem.2022.08.002.
14. Miao, Y., Ha, A., de Lau, W., Yuki, K., Santos, A.J.M., You, C., Geurts, M.H., Puschhof, J., Pleguezuelos-Manzano, C., Peng, W.C., et al. (2020). Next-Generation Surrogate Wnts Support Organoid Growth and Deconvolute Frizzled Pleiotropy In Vivo. Cell Stem Cell *27*, 840–851.e6. https://doi.org/10.1016/j.stem.2020.07.020.
15. Beumer, J., Puschhof, J., Yengej, F.Y., Zhao, L., Martinez-Silgado, A., Blotenburg, M., Begthel, H., Boot, C., van Oudenaarden, A., Chen, Y.-G., et al. (2022). BMP gradient along the intestinal villus axis controls zonated enterocyte and goblet cell states. Cell Rep. *38*, 110438. https://doi.org/10.1016/j.celrep.2022.110438.
16. Howitt, M.R., Lavoie, S., Michaud, M., Blum, A.M., Tran, S.V., Weinstock, J.V., Gallini, C.A., Redding, K., Margolskee, R.F., Osborne, L.C., et al. (2016). Tuft cells, taste-chemosensory cells, orchestrate parasite type 2 immunity in the gut. Science *351*, 1329–1333. https://doi.org/10.1126/science.aaf1648.
17. Beumer, J., Puschhof, J., Bauzá-Martinez, J., Martínez-Silgado, A., Elmentaite, R., James, K.R., Ross, A., Hendriks, D., Artegiani, B., Busslinger, G.A., et al. (2020). High-Resolution mRNA and Secretome Atlas of Human Enteroendocrine Cells. Cell *181*, 1291–1306.e19. https://doi.org/10.1016/j.cell.2020.04.036.
18. Wang, Y., Song, W., Wang, J., Wang, T., Xiong, X., Qi, Z., Fu, W., Yang, X., and Chen, Y.-G. (2020). Single-cell transcriptome analysis reveals differential nutrient absorption functions in human intestine. J. Exp. Med. *217*, e20191130. https://doi.org/10.1084/jem.20191130.
19. Fujii, M., Matano, M., Toshimitsu, K., Takano, A., Mikami, Y., Nishikori, S., Sugimoto, S., and Sato, T. (2018). Human Intestinal Organoids Maintain Self-Renewal Capacity and Cellular Diversity in Niche-Inspired Culture Condition. Cell Stem Cell *23*, 787–793.e6. https://doi.org/10.1016/j.stem.2018.11.016.
20. Hendriks, D., Artegiani, B., Hu, H., Chuva de Sousa Lopes, S., and Clevers, H. (2021). Establishment of human fetal hepatocyte organoids and CRISPR–Cas9-based gene knockin and knockout in organoid cultures from human liver. Nat. Protoc. *16*, 182–217. https://doi.org/10.1038/s41596-020-00411-2.
21. Artegiani, B., Hendriks, D., Beumer, J., Kok, R., Zheng, X., Joore, I., Chuva de Sousa Lopes, S., van Zon, J., Tans, S., and Clevers, H. (2020). Fast and efficient generation of knock-in human organoids using homology-independent CRISPR–Cas9 precision genome editing. Nat. Cell Biol. *22*, 321–331. https://doi.org/10.1038/s41556-020-0472-5.
22. Chen, Q., Shen, Y., and Zheng, J. (2021). A review of cystic fibrosis: Basic and clinical aspects. Anim. Models Exp. Med. *4*, 220–232. https://doi.org/10.1002/ame2.12180.
23. Beumer, J., and Clevers, H. (2021). Cell fate specification and differentiation in the adult mammalian intestine. Nat. Rev. Mol. Cell Biol. *22*, 39–53. https://doi.org/10.1038/s41580-020-0278-0.
24. van Es, J.H., van Gijn, M.E., Riccio, O., van den Born, M., Vooijs, M., Begthel, H., Cozijnsen, M., Robine, S., Winton, D.J., Radtke, F., et al. (2005). Notch/γ-secretase inhibition turns proliferative cells in intestinal crypts and adenomas into goblet cells. Nature *435*, 959–963. https://doi.org/10.1038/nature03659.
25. Bray, S.J. (2006). Notch signalling: a simple pathway becomes complex. Nat. Rev. Mol. Cell Biol. *7*, 678–689. https://doi.org/10.1038/nrm2009.
26. Ito, G., Okamoto, R., Murano, T., Shimizu, H., Fujii, S., Nakata, T., Mizutani, T., Yui, S., Akiyama-Morio, J., Nemoto, Y., et al. (2013). Lineage-Specific Expression of Bestrophin-2 and Bestrophin-4 in Human Intestinal Epithelial Cells. PLOS One *8*, e79693. https://doi.org/10.1371/journal.pone.0079693.
27. Yoo, Y.J., Kim, H., Park, S.R., and Yoon, Y.J. (2017). An overview of rapamycin: from discovery to future perspectives. J. Ind. Microbiol. Biotechnol. *44*, 537–553. https://doi.org/10.1007/s10295-016-1834-7.

28. Choi, J., Chen, J., Schreiber, S.L., and Clardy, J. (1996). Structure of the FKBP12-Rapamycin Complex Interacting with Binding Domain of Human FRAP. Science *273*, 239–242. https://doi.org/10.1126/science.273.5272.239.

29. Komor, A.C., Kim, Y.B., Packer, M.S., Zuris, J.A., and Liu, D.R. (2016). Programmable editing of a target base in genomic DNA without double-stranded DNA cleavage. Nature *533*, 420–424. https://doi.org/10.1038/nature17946.

30. Kanaya, T., Hase, K., Takahashi, D., Fukuda, S., Hoshino, K., Sasaki, I., Hemmi, H., Knoop, K.A., Kumar, N., Sato, M., et al. (2012). The Ets transcription factor Spi-B is essential for the differentiation of intestinal microfold cells. Nat. Immunol. *13*, 729–736. https://doi.org/10.1038/ni.2352.

31. Xiong, Z., Zhu, X., Geng, J., Xu, Y., Wu, R., Li, C., Fan, D., Qin, X., Du, Y., Tian, Y., et al. (2022). Intestinal Tuft-2 cells exert antimicrobial immunity via sensing bacterial metabolite N-undecanoylglycine. Immunity *55*, 686–700.e7. https://doi.org/10.1016/j.immuni.2022.03.001.

32. de Lau, W., Kujala, P., Schneeberger, K., Middendorp, S., Li, V.S.W., Barker, N., Martens, A., Hofhuis, F., DeKoter, R.P., Peters, P.J., et al. (2012). Peyer's Patch M Cells Derived from Lgr5+ Stem Cells Require SpiB and Are Induced by RankL in Cultured "Miniguts". Mol. Cell. Biol. *32*, 3639–3647. https://doi.org/10.1128/MCB.00434-12.

33. Ding, S., Song, Y., Brulois, K.F., Pan, J., Co, J.Y., Ren, L., Feng, N., Yasukawa, L.L., Sánchez-Tacuba, L., Wosen, J.E., et al. (2020). Retinoic Acid and Lymphotoxin Signaling Promote Differentiation of Human Intestinal M Cells. Gastroenterology *159*, 214–226.e1. https://doi.org/10.1053/j.gastro.2020.03.053.

34. von Moltke, J., Ji, M., Liang, H.-E., and Locksley, R.M. (2016). Tuft-cell-derived IL-25 regulates an intestinal ILC2–epithelial response circuit. Nature *529*, 221–225. https://doi.org/10.1038/nature16161.

35. Gerbe, F., Sidot, E., Smyth, D.J., Ohmoto, M., Matsumoto, I., Dardalhon, V., Cesses, P., Garnier, L., Pouzolles, M., Brulin, B., et al. (2016). Intestinal epithelial tuft cells initiate type 2 mucosal immunity to helminth parasites. Nature *529*, 226–230. https://doi.org/10.1038/nature16527.

36. Schneider, C., O'Leary, C.E., von Moltke, J., Liang, H.-E., Ang, Q.Y., Turnbaugh, P.J., Radhakrishnan, S., Pellizzon, M., Ma, A., and Locksley, R.M. (2018). A Metabolite-Triggered Tuft Cell-ILC2 Circuit Drives Small Intestinal Remodeling. Cell *174*, 271–284.e14. https://doi.org/10.1016/j.cell.2018.05.014.

37. Knoop, K.A., Kumar, N., Butler, B.R., Sakthivel, S.K., Taylor, R.T., Nochi, T., Akiba, H., Yagita, H., Kiyono, H., and Williams, I.R. (2009). RANKL Is Necessary and Sufficient to Initiate Development of Antigen-Sampling M Cells in the Intestinal Epithelium. J. Immunol. *183*, 5738–5747. https://doi.org/10.4049/jimmunol.0901563.

38. Lin, L., DeMartino, J., Wang, D., van Son, G.J.F., van der Linden, R., Begthel, H., Korving, J., Andersson-Rolf, A., van den Brink, S., Lopez-Iglesias, C., et al. (2023). Unbiased transcription factor CRISPR screen identifies ZNF800 as master repressor of enteroendocrine differentiation. Science *382*, 451–458. https://doi.org/10.1126/science.adi2246.

39. Kimura, S., Kobayashi, N., Nakamura, Y., Kanaya, T., Takahashi, D., Fujiki, R., Mutoh, M., Obata, Y., Iwanaga, T., Nakagawa, T., et al. (2019). Sox8 is essential for M cell maturation to accelerate IgA response at the early stage after weaning in mice. J. Exp. Med. *216*, 831–846. https://doi.org/10.1084/jem.20181604.

40. Kimura, S., Yamakami-Kimura, M., Obata, Y., Hase, K., Kitamura, H., Ohno, H., and Iwanaga, T. (2015). Visualization of the entire differentiation process of murine M cells: suppression of their maturation in cecal patches. Mucosal Immunol. *8*, 650–660. https://doi.org/10.1038/mi.2014.99.

41. Huang, L., Bernink, J.H., Giladi, A., Krueger, D., van Son, G.J.F., Geurts, M.H., Busslinger, G., Lin, L., Begthel, H., Zandvliet, M., et al. (2024). Tuft cells act as regenerative stem cells in the human intestine. Nature *634*, 929–935. https://doi.org/10.1038/s41586-024-07952-6.

42. Schneider, W.M., Chevillotte, M.D., and Rice, C.M. (2014). Interferon-Stimulated Genes: A Complex Web of Host Defenses. Annu. Rev. Immunol. *32*, 513–545. https://doi.org/10.1146/annurev-immunol-032713-120231.

43. Carthagena, L., Bergamaschi, A., Luna, J.M., David, A., Uchil, P.D., Margottin-Goguet, F., Mothes, W., Hazan, U., Transy, C., Pancino, G., et al. (2009). Human TRIM Gene Expression in Response to Interferons. PLOS One *4*, e4894. https://doi.org/10.1371/journal.pone.0004894.

44. Yu, K., Lujan, R., Marmorstein, A., Gabriel, S., and Hartzell, H.C. (2010). Bestrophin-2 mediates bicarbonate transport by goblet cells in mouse colon. J. Clin. Invest. *120*, 1722–1735. https://doi.org/10.1172/JCI41129.

45. Ameen, N., Alexis, J., and Salas, P. (2000). Cellular localization of the cystic fibrosis transmembrane conductance regulator in mouse intestinal tract. Histochem. Cell Biol. *114*, 69–75. https://doi.org/10.1007/s004180000164.

46. Liu, K., Zhang, X., Zhang, J.T., Tsang, L.L., Jiang, X., and Chan, H.C. (2016). Defective CFTR- β-catenin interaction promotes NF-κB nuclear translocation and intestinal in ammation in cystic fibrosis. Oncotarget *7*, 64030–64042. https://doi.org/10.18632/oncotarget.11747.

47. Frizzell, R.A., and Hanrahan, J.W. (2012). Physiology of Epithelial Chloride and Fluid Secretion. Cold Spring Harbor Perspect. Med. *2*, a009563. https://doi.org/10.1101/cshperspect.a009563.

48. Petri, W.A., Miller, M., Binder, H.J., Levine, M.M., Dillingham, R., and Guerrant, R.L. (2008). Enteric infections, diarrhea, and their impact on function and development. J. Clin. Invest. *118*, 1277–1290. https://doi.org/10.1172/JCI34005.

49. Wang, H., Zhong, Z., Luo, Y., Cox, E., and Devriendt, B. (2019). Heat-Stable Enterotoxins of Enterotoxigenic Escherichia coli and Their Impact on Host Immunity. Toxins *11*, 24. https://doi.org/10.3390/toxins11010024.

50. Weiglmeier, P.R., Rösch, P., and Berkner, H. (2010). Cure and Curse: E. coli Heat-Stable Enterotoxin and Its Receptor Guanylyl Cyclase C. Toxins *2*, 2213–2229. https://doi.org/10.3390/toxins2092213.

51. Fiskerstrand, T., Arshad, N., Haukanes, B.I., Tronstad, R.R., Pham, K.D.-C., Johansson, S., Håvik, B., Tønder, S.L., Levy, S.E., Brackman, D., et al. (2012). Familial Diarrhea Syndrome Caused by an Activating GUCY2C Mutation. N. Engl. J. Med. *366*, 1586–1595. https://doi.org/10.1056/NEJMoa1110132.

52. Rappaport, J.A., and Waldman, S.A. (2018). The Guanylate Cyclase C-cGMP Signaling Axis Opposes Intestinal Epithelial Injury and Neoplasia. Front. Oncol. *8*, 299. https://doi.org/10.3389/fonc.2018.00299.

53. Barton, J.R., Londregan, A.K., Alexander, T.D., Entezari, A.A., Bar-Ad, S., Cheng, L., Lepore, A.C., Snook, A.E., Covarrubias, M., and Waldman, S.A. (2023). Intestinal neuropod cell GUCY2C regulates visceral pain. J. Clin. Invest. *133*, e165578. https://doi.org/10.1172/JCI165578.

54. Dekkers, J.F., Wiegerinck, C.L., de Jonge, H.R., Bronsveld, I., Janssens, H.M., de Winter-de Groot, K.M., Brandsma, A.M., de Jong, N.W.M., Bijvelds, M.J.C., Scholte, B.J., et al. (2013). A functional CFTR assay using primary cystic fibrosis intestinal organoids. Nat. Med. *19*, 939–945. https://doi.org/10.1038/nm.3201.

55. Geurts, M.H., de Poel, E., Amatngalim, G.D., Oka, R., Meijers, F.M., Kruisselbrink, E., van Mourik, P., Berkers, G., de Winter-de Groot, K.M., Michel, S., et al. (2020). CRISPR-Based Adenine Editors Correct Nonsense Mutations in a Cystic Fibrosis Organoid Biobank. Cell Stem Cell *26*, 503–510.e7. https://doi.org/10.1016/j.stem.2020.01.019.

56. Busby, R.W., Bryant, A.P., Bartolini, W.P., Cordero, E.A., Hannig, G., Kessler, M.M., Mahajan-Miklos, S., Pierce, C.M., Solinga, R.M., Sun, L.J., et al. (2010). Linaclotide, through activation of guanylate cyclase C, acts locally in the gastrointestinal tract to elicit enhanced intestinal secretion and transit. Eur. J. Pharmacol. *649*, 328–335. https://doi.org/10.1016/j.ejphar.2010.09.019.

57. Braga Emidio, N., Tran, H.N.T., Andersson, A., Dawson, P.E., Albericio, F., Vetter, I., and Muttenthaler, M. (2021). Improving the Gastrointestinal Stability of Linaclotide. J. Med. Chem. *64*, 8384–8390. https://doi.org/10.1021/acs.jmedchem.1c00380.

58. Muanprasat, C., Sonawane, N.D., Salinas, D., Taddei, A., Galietta, L.J.V., and Verkman, A.S. (2004). Discovery of Glycine Hydrazide Pore-occluding CFTR Inhibitors. J. Gen. Physiol. *124*, 125–137. https://doi.org/10.1085/jgp.200409059.

59. Vanden Broeck, D., Horvath, C., and De Wolf, M.J.S. (2007). Vibrio cholerae: Cholera toxin. Int. J. Biochem. Cell Biol. *39*, 1771–1775. https://doi.org/10.1016/j.biocel.2007.07.005.

60. Hackley, C.R., Mazzoni, E.O., and Blau, J. (2018). cAMPr: A single-wavelength fluorescent sensor for cyclic AMP. Sci. Signal. *11*, eaah3738. https://doi.org/10.1126/scisignal.aah3738.

61. Wu, Y., Zeng, L., and Zhao, S. (2021). Ligands of Adrenergic Receptors: A Structural Point of View. Biomolecules *11*, 936. https://doi.org/10.3390/biom11070936.

62. Spellberg, B., and Edwards, J.E., Jr. (2001). Type 1/Type 2 immunity in infectious diseases. Clin. Infect. Dis. *32*, 76–102. https://doi.org/10.1086/317537.

63. Tsai, P.-Y., Zhang, B., He, W.-Q., Zha, J.-M., Odenwald, M.A., Singh, G., Tamura, A., Shen, L., Sailer, A., Yeruva, S., et al. (2017). IL-22 Upregulates Epithelial Claudin-2 to Drive Diarrhea and Enteric Pathogen Clearance. Cell Host Microbe *21*, 671–681.e4. https://doi.org/10.1016/j.chom.2017.05.009.

64. Ikpa, P.T., Sleddens, H.F.B.M., Steinbrecher, K.A., Peppelenbosch, M.P., de Jonge, H.R., Smits, R., and Bijvelds, M.J.C. (2016). Guanylin and uroguanylin are produced by mouse intestinal epithelial cells of columnar and secretory lineage. Histochem. Cell Biol. *146*, 445–455. https://doi.org/10.1007/s00418-016-1453-4.

65. Sawasvirojwong, S., Srimanote, P., Chatsudthipong, V., and Muanprasat, C. (2013). An Adult Mouse Model of Vibrio cholerae-induced diarrhea for Studying pathogenesis and Potential Therapy of Cholera. PLOS Negl. Trop. Dis. *7*, e2293. https://doi.org/10.1371/journal.pntd.0002293.

66. Bolick, D.T., Medeiros, P.H.Q.S., Ledwaba, S.E., Lima, A.A.M., Nataro, J.P., Barry, E.M., and Guerrant, R.L. (2018). Critical Role of Zinc in a New Murine Model of Enterotoxigenic Escherichia coli Diarrhea. Infect. Immun. *86*, e00183-18. https://doi.org/10.1128/IAI.00183-18.

67. van de Wetering, M., Francies, H.E., Francis, J.M., Bounova, G., Iorio, F., Pronk, A., van Houdt, W., van Gorp, J., Taylor-Weiner, A., Kester, L., et al. (2015). Prospective Derivation of a Living Organoid Biobank of Colorectal Cancer Patients. Cell *161*, 933–945. https://doi.org/10.1016/j.cell.2015.03.053.

68. Love, M.I., Huber, W., and Anders, S. (2014). Moderated estimation of fold change and dispersion for RNA-seq data with DESeq2. Genome Biol. *15*, 550. https://doi.org/10.1186/s13059-014-0550-8.

69. Butler, A., Hoffman, P., Smibert, P., Papalexi, E., and Satija, R. (2018). Integrating single-cell transcriptomic data across different conditions, technologies, and species. Nat. Biotechnol. *36*, 411–420. https://doi.org/10.1038/nbt.4096.

70. Pleguezuelos-Manzano, C., Puschhof, J., van den Brink, S., Geurts, V., Beumer, J., and Clevers, H. (2020). Establishment and Culture of Human Intestinal Organoids Derived from Adult Stem Cells. Curr. Protoc. Immunol. *130*, e106. https://doi.org/10.1002/cpim.106.

71. Ran, F.A., Hsu, P.D., Wright, J., Agarwala, V., Scott, D.A., and Zhang, F. (2013). Genome engineering using the CRISPR-Cas9 system. Nat. Protoc. *8*, 2281–2308. https://doi.org/10.1038/nprot.2013.143.

72. Andersson-Rolf, A., Mustata, R.C., Merenda, A., Kim, J., Perera, S., Grego, T., Andrews, K., Tremble, K., Silva, J.C.R., Fink, J., et al. (2017). One-step generation of conditional and reversible gene knockouts. Nat. Methods *14*, 287–289. https://doi.org/10.1038/nmeth.4156.

73. Uhlén, M., Fagerberg, L., Hallström, B.r.M., Lindskog, C., Oksvold, P., Mardinoglu, A., Sivertsson, Å., Kampf, C., Sjöstedt, E., Asplund, A., et al. (2015). Proteomics. Tissue-based map of the human proteome. Science *347*, 1260419. https://doi.org/10.1126/science.1260419.

74. Wijnakker, J.J.A.P.M., van Son, G.J.F., Krueger, D., van de Wetering, W.J., Lopez-Iglesias, C., Schreurs, R., van Rijt, F., Lim, S., Lin, L., Peters, P.J., et al. (2025). Integrin-activating Yersinia protein Invasin sustains long-term expansion of primary epithelial cells as 2D organoid sheets. Proc. Natl. Acad. Sci. USA *122*, e2420595121. https://doi.org/10.1073/pnas.2420595121.

75. Muraro, M.J., Dharmadhikari, G., Grün, D., Groen, N., Dielen, T., Jansen, E., van Gurp, L., Engelse, M.A., Carlotti, F., de Koning, E.J.P., et al. (2016). A Single-Cell Transcriptome Atlas of the Human Pancreas. Cell Syst. *3*, 385–394.e3. https://doi.org/10.1016/j.cels.2016.09.002.

76. Ding, J., Adiconis, X., Simmons, S.K., Kowalczyk, M.S., Hession, C.C., Marjanovic, N.D., Hughes, T.K., Wadsworth, M.H., Burks, T., Nguyen, L.T., et al. (2020). Systematic comparison of single-cell and single-nucleus RNA-sequencing methods. Nat. Biotechnol. *38*, 737–746. https://doi.org/10.1038/s41587-020-0465-8.

STAR★METHODS

KEY RESOURCES TABLE

REAGENT or RESOURCE	SOURCE	IDENTIFIER
Antibodies		
Rabbit anti-BEST4 antibody (polyclonal)	ATLAS antibodies	Cat# HPA058564; RRID: AB_2683759
Rabbit anti-Chromogranin A (CHGA) antibody (polyclonal)	Lab Ned	Cat# LN1401487; RRID: N/A
Rabbit anti-CA7 antibody (polyclonal)	Sigma-Aldrich	Cat# HPA047237; RRID: AB_2679994
Rabbit anti-GUCY2C antibody (monoclonal, clone# 2543C)	R&D Systems	Cat# FAB2157G; RRID: N/A
Mouse anti-BrdU antibody (monoclonal, clone# MoBU-1)	Thermo Fisher	Cat# B35128; RRID: AB_2536432
Alexa Fluor 488 donkey anti-rabbit	Thermo Fisher	Cat# A21206; RRID: AB_2535792
Alexa Fluor 647 donkey anti-mouse	Thermo Fisher	Cat# A31571; RRID: AB_162542
Alexa Fluor 647 donkey anti-rabbit	Thermo Fisher	Cat# A31573; RRID: AB_2536183
Chemicals, Peptides, and Recombinant Proteins		
BME (cultrex Basement Membrane Extract, growth factor reduced, type 2)	R&D Systems	Cat# 3536-005-02
adDMEM/F12 (advanced Dulbecco's Modified Eagle's Medium/F12)	Gibco	Cat# 12634028
P/S (Penicillin/Streptomycin)	Gibco	Cat# 15140122
HEPES	Gibco	Cat# 15630056
Glutamax	Gibco	Cat# 35050038
B-27 supplement	Thermo Fisher	Cat# 12587010
NAC (N-acetyl-L-cysteine)	Sigma-Aldrich	Cat# A9165
Noggin conditioned medium	U-Protein Express BV	Custom order
WNT surrogate	U-Protein Express BV	Custom order
EGF (human Epidermal Growth Factor)	Peprotech	Cat# AF-100-15
A83-01	Tocris	Cat# 2939
SB202190	Sigma-Aldrich	Cat# S7067
PGE2 (Prostaglandin E2)	Tocris	Cat# 2296
NIC (Nicotinamide)	Sigma-Aldrich	Cat# N0636
R-spondin1 conditioned medium	U-Protein Express BV	Custom order
IL-1β	Peprotech	Cat# 200-01B
IL-2	Peprotech	Cat# 200-02
IL-4	Peprotech	Cat# 200-04
IL-6	Peprotech	Cat# 200-06
IL-8	Peprotech	Cat# 200-08
IL-17A	Peprotech	Cat# 200-17
IL-17E (IL-25)	Peprotech	Cat# 200-24
IL-22	Peprotech	Cat# 200-22
IFN-α	Peprotech	Cat# 300-02AA
IFN-γ	Peprotech	Cat# 300-02
RANKL	Peprotech	Cat# 310-01C
TNF-α	Peprotech	Cat# 300-01A
BMP-2	Peprotech	Cat# 120-02C
BMP-4	Peprotech	Cat# 120-05ET
LPS (Lipopolysaccharides)	Sigma-Aldrich	Cat# L4391
Rapamycin	Selleckchem	Cat# S1039
DAPT	Sigma-Aldrich	Cat# D5942
Linaclotide	Targetmol Chemicals	Cat# T11852
GlyH-101	MedChemExpress	Cat# HY-18336

(*Continued on next page*)

Continued		
REAGENT or RESOURCE	SOURCE	IDENTIFIER
MYH-1485	MedChemExpress	Cat# HY-B0795
Doxycycline	Sigma-Aldrich	Cat# D1822
Norepinephrine (NE)	Sigma-Aldrich	Cat# A9512
Cholera toxin (CTX)	Sigma-Aldrich	Cat# C8052
5-Bromo-2'-deoxyuridine (BrdU)	Sigma-Aldrich	Cat# B5002
TrypLE (TrypLE™ Express Enzyme)	Thermo Fisher	Cat# 12605010
Opti-MEM™	Thermo Fisher	Cat# 31985070
Corning Cell Recovery Solution	Sigma-Aldrich	Cat# CLS354253
4% Formaldehyde solution	Sigma-Aldrich	Cat# 1.00496
DAPI (4',6-Diamidine-2'-phenylindole dihydrochloride)	Sigma-Aldrich	Cat# 10236276001
Critical Commercial Assays		
iQ™ SYBR Green Supermix	BioRad	Cat# 1708887
GoScript™ reverse transcriptase kit	Promega	Cat# A5000
Miniprep DNA isolation kit	Thermo Fisher	Cat# K210003
Midiprep DNA isolation kit	Thermo Fisher	Cat# K210005
EdU Assay kit	Thermo Fisher	Cat# C10337
NucleoSpin RNA kit	Macherey-Nagel	Cat# 740955.50
Deposited Data		
Single-cell RNA-sequencing dataset (Human intestinal organoid cells in "differentiation medium" +/- IFN-γ)	This paper	GEO: GSE242765
Experimental Models: Organoid lines		
Donor# P11N	van de Wetering[67]	Diakonessen Hospital Utrecht
Donor# 12339	He et al.[13]	The Netherlands Cancer Institute (NKI)
Donor# 3466N	He et al.[13]	NKI
Donor# 4403N	This paper	NKI
Oligonucleotides		
Sequences of qPCR primers, see Table S1	This paper	N/A
Sequences of sgRNAs, see Figures S1, S6, and S7	This paper	N/A
Recombinant DNA		
pSPgRNA	Addgene	plasmid# 47108
Frame-selector	Addgene	plasmid# 66940
mNeonGreen donor-targeting vector	Addgene	plasmid# 174092
P2A-tdTomato-BlastR donor-targeting vector	This paper	N/A
pCMV_AncBE4max_P2A_GFP	Addgene	plasmid# 112100
p2T-SPIB-overexpression vector	This paper	N/A
Software and Algorithms		
Graphpad PRISM 6	Graphpad software	https://www.graphpad.com
Adobe Photoshop (CC2017)	Adobe	https://www.adobe.com/products/photoshop.html
Adobe Illustrator (CC2017)	Adobe	https://www.adobe.com/products/illustrator.html
Biorender	Biorender	http://www.biorender.com
IMARIS (v9.3)	IMARIS	https://imaris.oxinst.com
Rstudio (v3.6.3)	Rstudio	https://www.rstudio.com
Flow Jo (vX)	Flow Jo	https://www.flowjo.com
DEseq2 R package	Love et al. [68]	http://www.bioconductor.org/packages/release/bioc/html/DESeq2.html
Seurat R package v3	Butler et al. [69]	http://satijalab.org/seurat/

EXPERIMENTAL MODEL AND STUDY PARTICIPANT DETAILS

Human intestinal organoid lines

A total of four human intestinal organoid lines were established previously in our lab and recruited in this study.[13,67] Human ileum tissues (Donor# 12339, 3466N and 4403N) were obtained from the Netherlands Cancer Institute (NKI), and colon tissue (Donor# P11N) was obtained from the Diakonessen Hospital Utrecht, with informed consent from each patient. The study was approved by the ethical committee and was conducted in accordance with the Declaration of Helsinki and Dutch law. This study complied with all relevant ethical regulations regarding research involving human participants.

METHOD DETAILS

Organoid culture and differentiation

Organoid expansion: Human intestinal organoids were mixed with BME, seeded as 5–10 μl droplets, kept in expansion medium and passaged weekly by mechanic dissociation as described previously.[70] The expansion medium consisted of adDMEM/F12 supplemented with 100 U/ml P/S, 10 mM HEPES, 1× Glutamax, 1× B-27 supplement, 1.25 mM NAC, 1% (v/v) recombinant Noggin, 0.5 nM WNT surrogate, 50 ng/ml EGF, 0.5 μM A83-01, 1 μM SB202190, 1 μM PGE2, 10 mM NIC and 20% (v/v) RSPO1. The culture medium was refreshed every 2-3 days.

Organoid differentiation: Organoids cultured in expansion medium for 4-5 days were subjected to differentiation. Therefore, the expansion medium was completely removed and, to wash out the remaining growth factors, the organoids were incubated in 3 ml adDMEM/F12 supplemented with 100 U/ml P/S, 10 mM HEPES and 1× Glutamax for 2 hours. Then organoids were cultured in differentiation medium for 6-8 days. Differentiation medium was prepared by removing EGF, Noggin, SB202190, A83-01, WNT surrogate, PGE2 and NIC from expansion medium.

Other factors and small molecules used in this study: Interleukins and interferons were used at 10 ng/ml, RANKL was used at 100 ng/ml, TNF-α was used at 20 ng/ml, BMP-2 and BMP-4 were used at 50 ng/ml, LPS was used at 100 ng/ml, rapamycin was used at 1 μM, DAPT was used at 10 μM, MYH-1485 was used at 10 μM, doxycycline was used at 1 μg/ml, linaclotide was used at 10 μM, cholera toxin was used at 1 μg/ml, norepinephrine was used at 10 μM, GlyH-101 was used at 50 μM.

Generation of genetically modified organoids

Preparation of cells for electroporation: Intestinal organoids cultured in expansion medium for 4-5 days were dissociated into small cell clumps with 1 ml TripLE at 37 °C for 4 mins, followed by gently pipetting 20 times. After TripLE dissociation, the cell suspension was filtered through a 40 μm cell strainer, washed twice with cold Opti-MEM™ and re-suspended in Opti-MEM™ for electroporation.

Preparation of sgRNA plasmid: sgRNAs, targeting different genes, were cloned into pSPgRNA vector (Addgene, plasmid# 47108) according to the previously described protocol.[71] The sgRNA sequences used in this study can be found in Figures S1, S6, and S7.

CA7-P2A-tdTomato, *SPIB-P2A-tdTomato* and *MUC2-mNeonGreen* knockin reporter organoids were generated using the CRISPR-HOT approach.[20,21] The frame-selector plasmid containing an sgRNA (to linearize the donor-targeting vector), *Cas9* and *mCherry* (for the detection and FACS sorting of the successfully transfected cells) was obtained from Addgene (plasmid# 66940). The *mNeonGreen* donor-targeting vector was obtained from Addgene (plasmid# 174092). The *P2A-tdTomato-BlastR* donor-targeting vector was a modification of the Addgene plasmid# 138568, by replacing the *Clover* sequence with *tdTomato*. 5 μg sgRNA plasmid, 5 μg frame-selector plasmid and 5 μg donor-targeting vector were co-transfected into organoid cells using the NEPA electroporation system (NEPAGENE). After FACS sorting, based on the mCherry fluorescence, followed by blasticidin selection, subclones were picked and expanded in expansion medium. Successful insertions were first identified by direct visualization of the fluorescence marker in the differentiated organoids, and then confirmed by targeted genotyping via Sanger sequencing (Figures S1B, S6, and S7). Knockin of the reporter cassette doesn't change the coding sequence of *MUC2*, *CA7* and *SPIB*. Of note, we did not find significant differences in the cell viability (Figures S5M and S5N), mRNA levels of BEST4/CA7$^+$ cell markers (Figure S6A), or numbers of BEST4/CA7$^+$ cells (Figure S6B) between the WT and reporter organoids.

CHGA-IRES-iRFP670 knockin reporter organoids were generated and described in previous studies.[13,38]

CRISPR C-to-T base-editing[29] was used to generate *SPIB, CA7, BEST4 and GUCY2C* knockout organoids (by introducing an early stop codon): 7.5 μg pCMV_AncBE4max_P2A_GFP plasmid (Addgene, plasmid# 112100), 2.5 μg sgRNA plasmid and a two-plasmid transposon system[72] (5 μg PiggyBac transposase plasmid + 5 μg donor plasmid with terminal inverted repeats (TIRs) bearing hygromycin resistance for organoid selection) were co-transfected into organoid cells through electroporation. After FACS sorting of live single cells followed by hygromycin selection, subclones were picked and expanded in expansion medium. Successful homozygous knockout organoids were confirmed by targeted genotyping via Sanger sequencing (Figure S7).

To generate *SPIB*-overexpressing organoids, the transgenic constructs, including *SPIB-IRES-EGFP* (driven by TRE3GS promoter) and Tet-ON 3G transcription factor (driven by CMV promoter), were cloned into a p2T vector, flanked by 3' and 5' Tol2 sequences. Integration of these transposable elements into cell genome was mediated by mT2TP transposase. The cAMPr sensor[60] construct (driven by CAGGS promoter) was introduced into the reporter organoids using the same strategy.

Immuno-staining and confocal imaging

Organoids were released from BME using ice-cold Corning Cell Recovery Solution and fixed in 4% formaldehyde solution at room temperature for 1 hour, followed by 3 times of washing with PBS (phosphate buffered saline), and then blocked with the whole-mount blocking buffer at room temperature for 1 hour. Blocking buffer was 10% FBS (fetal bovine serum) in PBS-T (PBS with 0.1% TritonX-100). Primary antibodies were diluted in blocking buffer and incubated overnight at 4 °C. After 3 times of washing with PBS-T, secondary antibodies and DAPI were diluted in blocking buffer at 1:1000, and incubated overnight at 4 °C. Organoids were then 3 times washed with PBS-T and mounted for confocal imaging. A Leica SP8 confocal detection system fitted on a Leica DMi8 microscope captured the images. For image processing, maximum-projection of Z-stack images were performed using Leica LAS X software. We directly used the original images exported by Leica LAS X software, with minimal processing, such as simple rotating or cropping (for display purposes). The numbers of BEST4/CA7$^+$ cells per organoid were manually counted.

Primary antibodies used in this study: rabbit anti-BEST4 antibody was used at 1:500; rabbit anti-CHGA antibody was used at 1:5000; rabbit anti-CA7 antibody was used at 1:200; rabbit anti-GUCY2C antibody was used at 1:50; mouse anti-BrdU antibody was used at 1:100.

Immunohistochemistry (IHC) staining images of CFTR and GUCY2C in primary human small intestine tissues were all derived from the Human Protein Atlas (https://www.proteinatlas.org/).[73]

Live cell tracking

To trace the generation of CA7-tdTomato$^+$ cells (w/wo IFN-γ treatment), the reporter organoids were cultured in differentiation medium for 48 hrs (when most of the organoid cells were tdTomato$^-$) or 72 hrs (when many tdTomato$^+$ cells were generated in the IFN-γ-treated group). These organoids were then staged on the Leica SP8 confocal detection system fitted on a Leica DMi8 microscope (equipped with a CO_2 and temperature control system) to capture time-series images with z-stacks every 30 mins for 24 hours. 3D images were generated and analyzed using the IMARIS software.

Nucleotide pulse-chase experiment and EdU/BrdU labeling

The nucleotide pulse-chase experiment was performed by labeling stem/TA cells with BrdU during the expansion stage for 2 days, just before differentiation. EdU, together with or without IFN-γ, was then added from differentiation day 1 for a total of 4 days. Organoids were then fixed, and EdU color development was conducted following the manufacturer's protocol. BrdU antibody staining followed the protocol described above.

Imaging of cAMP sensor

BEST4/CA7$^+$ cells (CA7-tdTomato$^+$) were FACS-sorted, plated in glass-bottom imaging plates (coated with Invasin protein for quick attachment[74]), and cultured in differentiation medium overnight for attachment. The cells were then staged on the Leica SP8 confocal detection system fitted on a Leica DMi8 microscope (equipped with a CO_2 and temperature control system) to capture time-series images with z-stacks every 180 secs for 30 mins. Cholera toxin (CTX) was added 10 mins before imaging. The fluorescence intensity of cAMP sensor was measured using the Leica LAS X software and normalized to the fluorescence intensity at t=0 min (set as 1.0).

Sample preparation and flow cytometry

Organoids were dissociated with 1 ml TripLE at 37 °C for 6-8 mins, followed by gently pipetting 20 times. After TripLE dissociation, the cell suspension was filtered through a 40 μm cell strainer and stained with DAPI for FACS analysis or cell sorting. Samples were analyzed on a BD LSR Fortessa X20 equipped with 4 lasers (BD Bioscience). Cell sorting was performed on a BD FACS Influx cell sorter equipped with 5 lasers (BD Bioscience). At least 5,000 DAPI$^-$ live cells were recorded for each analyzed sample. The percentage of fluorescence$^+$ cells within the total DAPI$^-$ live cells were quantified and shown in the figures.

Sample preparation for scRNA-seq analysis

Differentiated organoids were dissociated into single cells for FACS sorting as described above. Single, DAPI$^-$ live cells were sorted, based on the fluorescence levels, on a BD FACS Influx cell sorter. Individual single cells were collected in 384 well-plates containing ERCC spike-ins (Agilent), reverse transcription primers (Promega) and dNTPs (Promega) as previously described.[15,17] 384 cells were collected for each culture condition (Ctrl v.s. IFN-γ). To enrich the BEST4/CA7$^+$ cells, tdTomato$^-$ cells (representing BEST4/CA7$^-$ cell lineages) and tdTomato$^+$ cells (representing BEST4/CA7$^+$ cells) were sorted at a 1:3 ratio in cell numbers. Single-cell RNA-sequencing was performed according to the SORT-seq, a 384-well plate-based, robotized version of CEL-seq2 method.[75] Sequencing libraries were generated with TruSeq small RNA primers (Illumina) and sequenced on the Illumina NextSeq platform. Sequencing reads were mapped to the human GRCh38 genome to generate the gene expression matrix for further scRNA-seq analysis.

Analysis of organoid scRNA-seq datasets

Cell filtering: We used the Seurat R package (v3) for data integration, analysis and visualization,[69] according to a standard workflow described by Satija Lab (Codes are available at https://satijalab.org). To create Seurat objects, genes expressed in at least one cell and cells with at least 1,000 detected genes were selected. Notably, we did not filter out cells based on the mitochondrial ratio, as the

CEL-seq2 method significantly increases the sensitivity for gene detection but also yields a higher mitochondrial ratio compared to other platforms, such as 10X chromium, as noted in a previous side-by-side comparison study.[76] The overall mitochondria ratio in our datasets is around 40% (Figure S1H).

Data normalization and PCs selection: After creating the Seurat objects, data normalization was performed based on "LogNormalize" method, with the "scale.factor" set to 10,000. Variable features were found by the "vst" method. The top 2,000 differentially expressed genes (DEGs) were selected for principal component (PC) analysis. The top 20 PCs were used for dataset integration.

Dimensional reduction, cell clustering and data display: Dimensional reduction was performed using the Uniform Manifold Approximation and Projection (UMAP) method. Cell clustering was based on the shared-nearest neighbor (SNN) method with the resolution set to 0.6. A total of 6 cell clusters were identified. After cell type annotation, based on the well-known intestinal cell type markers, 2 clusters with unclear cellular identity, were removed from further analysis and data display. Violin plots, heatmap, dot plots and individual UMAP plots for the given genes were generated by the Seurat toolkit functions VlnPlot, DoHeatmap, DotPlot and FeaturePlot, respectively.

To get the DEGs between Ctrl and IFN-γ-induced BEST4/CA7$^+$ cells, the raw counts data was subjected to DEseq2 R package[68] and analyzed with default settings. DEGs were defined by $|\log_2(\text{fold change})| \geq 0.585$ with adjusted p-value ≤ 0.01.

Analysis of primary intestinal scRNA-seq datasets

Four published datasets were integrated using Seurat R package (v3). To create the Seurat objects, in GEO: GSE119969[19] and GEO: GSE125970[18] datasets, genes expressed in at least 3 cells and cells with at least 200 detected genes were selected, in GEO: GSE146799[17] dataset, genes expressed in at least 3 cells and cells with at least 1,000 detected genes were selected. We directly used the Seurat object provided by Elmentaite et al.,[2] but only selected the adult and pediatric healthy cells for our analysis. In addition, we removed the TA cells and enterocytes from Elmentaite et al. dataset to accelerate the speed of analysis. The other three datasets still contain sufficient numbers of these cells for analysis.

Data normalization was performed based on "LogNormalize" method, with the "scale.factor" set to 10,000. Variable features were found by the "vst" method and the top 2,000 DEGs were selected for PC analysis. The top 30 PCs were selected for dataset integration. Dimensional reduction was performed using UMAP method, while the cell clustering was based on the SNN method. After cell type annotation, based on the well-known intestinal cell type markers, we only used the cells with a clear cellular identity for further analysis and data display.

Comparisons between organoid and primary BEST4/CA7$^+$ cells: BEST4/CA7$^+$ cells and enterocytes from organoid and primary cell datasets were integrated based on the top 20 PCs, and visualized in the UMAP plots. Cell clustering was based on SNN method with the resolution set to 0.03, which identified two cell clusters representing the BEST4/CA7$^+$ cells and enterocytes, respectively.

RNA extraction and qPCR

Organoids or FACS-sorted cells were subjected to RNA isolation using a NucleoSpin RNA kit following the manufacturer's protocol. Reverse transcription reactions were performed using GoScript^{TM} reverse transcriptase kit. cDNA was subjected to qPCR analysis using iQ^{TM} SYBR Green Supermix on a CFX Connect Real-Time PCR machine (BioRad). For gene expression analysis, qPCR was performed with gene-specific qPCR primers. Ct value of each gene was normalized to the housekeeping gene GAPDH (as the ΔCt), and fold change between experimental groups was calculated with the $2^{-\Delta\Delta Ct}$ method. All qPCR primers used in this study are listed in Table S1.

Organoid swelling assay

Live organoids were staged on the Leica SP8 confocal detection system fitted on a Leica DMi8 microscope (equipped with a CO_2 and temperature control system) to capture time-series images every 15 mins for 3 hours. To induce organoid swelling, 10 μM linaclotide or 1 μg/ml cholera toxin was added immediately before live imaging. To block organoid swelling, 10 μM norepinephrine (NE) or 50 μM CFTR inhibitor GlyH-101 was added 3 hours before imaging. To quantify the volume of the organoid lumen, the length and width of lumen were measured, and the volume was calculated using the following formula: volume = $4/3\pi \times (\text{length}/2) \times (\text{width}/2)^2$. Then, the relative volume at t=180 min was normalized to the volume at t=0 min (set as 1.0).

QUANTIFICATION AND STATISTICAL ANALYSIS

Data were presented as mean ± SD (Standard Deviation) to indicate the variation. Student's t test was used when two experimental groups were compared. One-way ANOVA was used when multiple experimental groups were compared. All the p values were calculated using Graphpad PRISM 6 with the following significance: n.s. p>0.05, * p<0.05, ** p<0.01, *** p<0.001, **** p<0.0001. The statistical details for each experiment can be found in the figures and figure legends.